Exploration of new steerable mechanism for stiff handheld minimally invasive surgery instrument

By

R.M.G.P. van Bodegom

in partial fulfilment of the requirements for the degree of

Master of Science

in Mechanical Engineering

at the Delft University of Technology,

to be defended publicly on Tuesday February 28, 2017 at 14:00 PM.

Supervisor:	Prof. dr. ir. P. Breedveld	TU Delft
Thesis committee:	Ir. P. Henselmans	TU Delft
	Dr. ir. D.H. Plettenburg	TU Delft

Abstract

Background: Minimally Invasive Surgery (MIS) gained increasing support in the surgical community over the last decades. Due to the rigid tip of current used rigid instruments the maneuverability is limited during a procedure. To increase maneuverability steerable instruments have been developed. However current handheld steerable instruments contain low bending stiffness, which is one of the reasons that these instruments are hardly used in clinical practice. This study aims to design and evaluate a new stiff steerable mechanism with 2 Degrees Of Freedom (DOF) for use in a handheld MIS instrument.

Methods: Characteristics of the steering mechanisms were described and analyzed. The most suited approach for creating a stiff steerable mechanism was selected. Multiple 2 DOF stiff concepts were designed. Of these, three concept prototypes (scaled $10mm$) were engineered and manufactured (3D printing). The ability to steer and the stiffness of the prototypes was evaluated. In addition, the most promising mechanism was redesigned to fit the required $5mm$ dimensions. It's robustness was verified using Finite Element Method (FEM) techniques.

Results: Eight different mechanisms were described and analyzed. The most suited approach is a mechanism that consists of solid rods and universal joints to guide steering forces from handle to tip and external forces from tip to handle. Five concepts were designed that enable a parallel motion of which three were developed further in $10mm$ scale prototypes. Preliminary results showed an increase in stiffness of a factor $2{,}7$ compared to existing instruments. The real scale implementation study resulted in a $5mm$ version of the mechanism that is capable of guiding the forces required to drive all the functionalities of a MIS instrument (steering, grasping).

Conclusion: It can be concluded that a $5mm$ steerable MIS instrument with a stiff tip is feasible. The mechanism contains a cardan mechanism and axially moving rods that slide over a special constructed surface. The scaled prototype provided at least $2{,}7$ times higher stiffness compared to existing instruments.

1 Introduction

Over the last decades Minimally Invasive Surgery (MIS) gained increasing support. Advantages of MIS procedures compared to open surgery were described as reasons for this increased support [1],[2]. One of these is the reduced affected region as the procedure takes place through one or more small incisions instead of via one large incision. This results in a lower risk of infections and therefore the recovery time of the patient will be shorter. However currently applied instruments have a limited maneuverability as the tip is rigidly fixed to the shaft. Therefore the surgeon is only able to move inwards and outwards, pivot around the insertion point and rotate the instrument [3].

To overcome the lack of maneuverability steerable MIS instruments were developed. A steerable instrument is able to bend the tip, preferably in two Degrees Of Freedom (DOF). While the tip is made bendable, stiffness of the tip often reduces. If a surgeon wants to perform a task in which high forces are exerted on the tip, for example during suturing, the tip may not deviate from the intended position. Deviation of the tip can lead to inaccuracy during handling of the instrument which can lead to dangerous situations as it could cause unintended damage.

State of the art

From the literature review was found that a stiff steerable MIS instrument consists of one or multiple frame elements and an actuation mechanism [4]. Frame elements can be permanent stiff or made stiff by the use of an additional stiffening mechanism. It was concluded that using these approaches both the stiffness and steer ability of the mechanism are determined by the compliance of the frame. Besides the use of the frame elements to obtain stiffness, stiffness can also be increased by locking the actuation mechanism. In this case stiffness is determined by compliancy of both the actuation mechanism and locking mechanism.

Handheld steerable MIS instruments are not applied much in clinical use yet. The Covidien SLIS Clinch displayed in Figure 1.1 is one of the few that is commercially available. This instrument is steered by four cables which are attached to the tip and handle. By steering the handle cables are pulled and with that the tip is steered. Fixation of the instrument is performed by fixating the proximal bending section in the steered position. A different instrument which is widely used, however not handheld, is the Endowrist used in the Da Vinci robotic surgical system. To steer the tip, Endowrist illustrated in Figure 1.2 uses a combination of cables and pulleys. Stiffness is generated by tension in the actuation cables. External forces applied to the tip of the instrument will therefore be resisted by the cables. Due to small radii of the pulleys in combination with high tension forces in the cables, cable fatigue occurs. As a result the lifespan is limited to ten MIS procedures [7].

Problem definition

Currently available handheld MIS instruments provide a low stiffness of the tip. This is one of the reasons that handheld steerable instruments are not widely applied in clinical use. Most current developed instruments that are stiff possess a high level of complexity which makes the instrument more vulnerable for failure and complicates assembly.

Goal of the study

Explore a new, two degrees of freedom, steering mechanism providing stiff steering for use in a handheld minimally invasive surgery instrument that is simple and robust.

Layout of the study

To achieve this goal, at first requirements of the instrument were determined in chapter two.

Figure 1.1 - Impression of the Covidien SILS Clinch handheld steerable instrument. Image adopted from Medtronic. [5]

Figure 1.2 - Cable driven steerable instrument Endowrist developed by Intuitive Surgical [6]. Image adopted from Intuitive Surgical

According to these requirements the most suited approach to create a stiff steerable instrument was selected. Design concepts were generated utilizing the selected approach in chapter three. Three concepts were developed further in proof of concept prototypes described in chapter four. Proof of concept prototypes were tested on steerability and stiffness in chapter five. Test results were evaluated in chapter six. Chapter seven describes a study performed to verify the applicability of the mechanism in a $\emptyset\, 5mm$ instrument design. Results were discussed in the discussion and conclusions were drawn in chapters eight and nine. Recommendations for future work were addressed in chapter ten.

Requirements of the mechanism

This thesis describes the design of a new stiff steering mechanism for use in a handheld steerable MIS instrument. Handheld Steerable instruments can be used directly in MIS procedures in which rigid instruments are currently applied. No further adaptations to the procedure or other equipment is required. This in contrary to the implementation of a robotic surgical system, like the Da Vinci surgical system, which requires a large investment of the hospital and the procedure must be adapted to the abilities of the system.

In order to evaluate different steering approaches first the steerable MIS instrument was evaluated. A steerable MIS instrument consist of five basic components as shown in Figure 1.3. The tip of the instrument is equipped with a specific tool designed to perform the intended task. The distal bending section enables steering of the tip. The shaft houses transmission elements which transfer forces generated by a torque at tip to the handle. The shaft also aligns tip and handle with respect to transmission elements. Transmission elements transfer the steering motion from handle to tip. The proximal bending section enables steering of the handle. The handle is operated by the user and controls functionalities like steering, opening and closing of the tip. As a result of the required dimensions of the instrument the transmission elements will be long and thin.

During MIS procedures $5mm$ trocars are used through which the instrument is inserted in the human body. To ensure that the instrument will fit through the trocar the outer diameter of the tip and shaft of the instrument is restricted to maximal $\emptyset\, 5mm$. The shaft of the instrument has a typical length of $300mm$.

All functionalities of the instrument should be operated using one hand. During tasks like suturing the surgeon applies two instruments at the same time, one in each hand. For efficient and successful fulfillment of the task it is not preferred that the surgeon is required to use both hands in order to fixate the position of one instrument for example.

The tip of the instrument is required to steer in two DOF. It is a wish to achieve a large steering angle in all directions however a steering angle of 45 degrees is required..

The instrument should have a bending stiffness of the tip which is at least greater than stiffness achieved in current developed handheld steerable MIS instruments. To obtain a good comparison the Covidien SILS Clinch will be tested according to the same test procedure.

Described characteristic were converted into design requirements. An overview of the requirements is displayed in Figure 1.4.

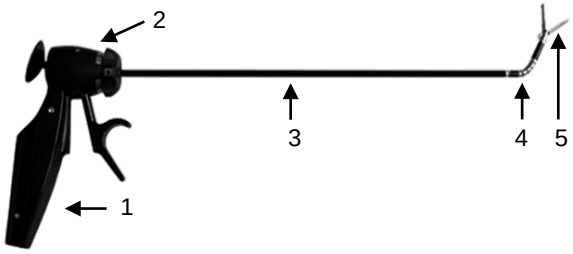

Figure 1.3 - Overview of elements of a steerable MIS instrument. 1: handle, 2: proximal bending, 3: shaft, 4: distal bending, 5: tip Displayed instrument: Miflex. Image adopted from [8]

Category	Requirement/Wish
Type of mechanism	**Requirement:** Handheld instrument
Usability	**Requirement:** Steering of the instrument should be performed using one hand.
Dimensions	**Requirement:** Maximal outside diameter of tip Ø5mm
Dimensions	**Wish:** Length of the shaft 30cm
Stiffness	**Requirement:** The tip of the mechanism should be stiffer than current developed steerable instruments
Range of motion	**Requirement:** Instrument is steerable in 2 Degree Of Freedom.
	Requirement: Steering angle in both DOF of 45 degrees from the center in all directions.

Figure 1.4 - Overview of the requirements of the instrument

2 Engineering approach

To select the most suitable engineering approach, first an analysis of the mechanism was performed. Based on the analysis different approaches to obtain maximal stiffness were described and evaluated. Finally the most suitable approach was chosen.

Bending sections of the mechanism consist of the steering mechanism. This mechanism can be designed fully actuated and under actuated. Based on an evaluation of a fully actuated instrument prototype and two under actuated instruments was concluded that a fully actuated joint mechanism shows significant larger bending stiffness compared to an under actuated joint mechanism [9]. Based on these results, it was chosen to apply a fully actuated joint construction for steering of the instrument.

Force analysis

Stiffness of the instrument is determined by the weakest element in the mechanism. Evaluation of the instrument shows that forces will be transferred from the tip to the handle via the joints and the transmission elements. Evaluation of the sensitivity of the elements was performed by first executing a force analysis of the mechanism.

A schematic representation of the elements which transfer force is displayed in Figure 2.1. The dark grey element represents a transmission element whereas light grey elements represent the handle and tip joints. The dot is the rotation point of the joint and is fixed with respect to the frame.

A closer look at the joint element indicates the ratio in forces between the external force F_e and the transmission force F_t. If external force is applied at $r_e = 15mm$ and the distance r_t between rotation point and F_t is $1mm$ the ratio is 15. To obtain a torque of for example $250Nmm$ an external force $F_e = 16.67N$ results in a force $F_t = 250N$ in the transmission element. Note that in this example only one transmission element was applied to compensate the external force. Because transmission elements were long, thin and experience the highest forces these elements were indicated as most vulnerable elements in the mechanism. Therefore these elements will to great extend determine the stiffness of the mechanism.

The Load Displacement Equation (2.1) showed that a larger surface A results in a smaller axial displacement [10].

$$\delta = \frac{P \cdot L}{A \cdot E} \qquad (2.1)$$

Based on the analysis was concluded that stiffness of the mechanism highly depends on stiffness of transmission elements. A thicker transmission element results in a smaller deformation of the transmission elements. Therefore thickness of the transmission elements is preferably maximized.

Types of transmission elements

Different types of transmission elements were distinguished. These comprise flexible, hydraulic / pneumatic and solid transmission elements as shown in Figure 2.2. First a description of each category is given, afterwards the most promising transmission element type was selected. As the mechanism will be applied in a handheld mechanism robot assisted or electronic actuated mechanisms were not evaluated. Mechanisms containing magnetic elements were not evaluated as these probably affect the performance of other instruments or will be affected by other instruments during the procedure.

Flexible transmission elements encompass cable driven mechanisms. To apply cables to steer the mechanism, a bending radius of the cable is required. For a MIS instrument this bending radius is limited as the dimensions of the instrument are restricted. Moreover, steering cables can only be applied to pull.

Pneumatic transmission elements are for example applied by Zhao in the mechanism shown in Figure 2.2 [12]. The mechanism contains three parallel placed columns of chambers in series which can be pressurized. While applying different pressure in the columns, the mechanism is able to steer. By increasing pressure in all columns the stiffness of the mechanism increases.

Solid transmission elements comprise mechanisms in which rods and joints are applied. Rods can be applied to push or pull to transfer the motion and forces from the tip to the handle and vice versa. Joints which convert the movement of the rod in

Figure 2.1 - Force analysis of steering mechanism. Dark grey element represent the transmission and in light grey the joints. The blue point indicates the rotation point of the joint.

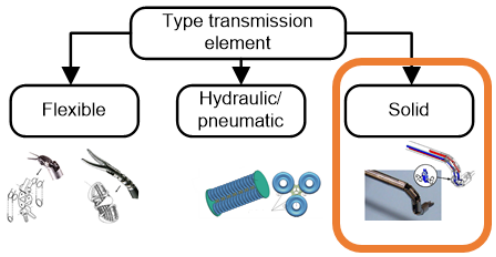

Figure 2.2 - Overview of types of transmission elements. Images adopted from [11] (left image), [12] (middle) and [13] (right image)

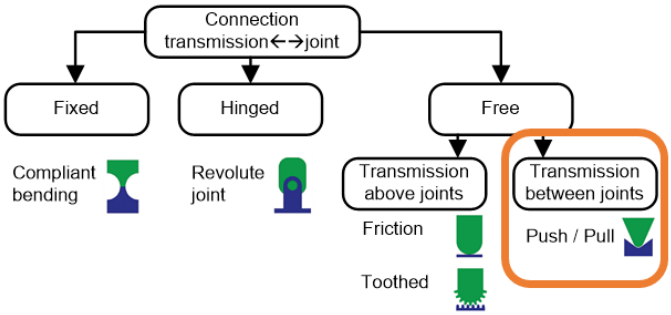

Figure 2.3 - Schematic overview of connections types between the transmission element and joint. Transmission element represented in green and joint in blue. Images adopted from [14].

rotation of the tip will transfer all forces and are difficult to minimize to fit in a $\emptyset 5mm$ mechanism. For increasing the bending stiffness the rod can be created with a specific shape in which the rod is supported and bending of the rod is prevented.

Selection type of transmission element

Evaluation of all three types of connection elements leads to the following observations. To maximize stiffness of the cable used in the flexible transmission elements approach, thickness should be maximized. However a thicker cable requires a larger bending radius which is restricted by the dimensions of the instrument. Therefore thin cables are required to enable steering with a small bending radius.

To increase stiffness tension in cables can be increased. However in combination with the small bending radius this results in increased fatigue of the cables. For this reason the Robot assisted cable driven instrument Endowrist, shown as an example in Figure 2.2, has a maximal lifetime of 10 procedures [7]. An evaluation of cable driven instruments Dragonflex, LaparoAngle and Miflex performed by Jelinek et al. resulted in a displacement of at least $0{,}4mm$ while a torque of $30Nmm$ was applied at the tip [9].

The described pneumatic transmission element approach was evaluated with an FEM analysis from which was found that while pressurized at $0{,}2MPa$ a force of $0{,}2N$ at the top ($15mm$) resulted in a horizontal displacement of $7{,}74mm$. The mechanism had diameter of $9mm$. Next to the low stiffness challenges arise if the mechanism is scaled down to implement in a 5mm design as the size of the chambers and connections become very small. A very precise control of the pressure is required to be able to steer and stiffen the mechanism. Therefore the mechanism becomes complex.

Application of rods does not require a bending radius. A mechanism consisting of rods can be designed in which the thickness of the rods can be maximized to enable maximal stiffness of the transmission elements. The performance of a mechanism which applies solid transmission elements greatly depends on the connection of the solid elements with the joints. In a current design, shown in Figure 2.2, very small hinges were applied which are difficult to miniaturize.

According to this evaluation was chosen to use solid transmission elements to create a stiff steerable MIS instrument as this has the highest potential to create stiff steerable transmission elements implemented in a 5mm diameter instrument. Compared to the other types of transmission elements was found that solid elements can be made more robust as no bending radius is required. Complexity is low compared to a hydraulic or pneumatic mechanism in which a complex stiffening mechanism should be applied. The risk of failure is lower as no complex elements or elements with a high risk of fatigue were required.

Connection transmission and joint

Application of rods requires that the connection between the rods and joints is able to withstand the forces while enabling the steering motion. The connection with the joints is therefore of great influence on total stiffness. Figure 2.3 shows an abstract overview of possible connections containing fixed, hinged and free connections. The transmission element is represented in green whereas the joint is blue. Application of the connection types in the mechanism will result in a different design however the applied principles are equal to the ones shown in Figure 2.3.

Fixed connections can be established by compliant elements. For the instrument this results in one part combining rods and joints with reduced thickness at the transition point between rod and joint to enable

rotation of the rods. However one of the characteristics of a compliant element is that energy is stored when bended from the preferred position. Therefore the mechanism will always move back to the preferred position. Continuous input is required to maintain the steered position.

Hinged connections are used in the example for solid transmission elements shown in Figure 2.2. Evaluation of the mechanism shows that to enable steering in two DOF multiple rods and hinges are connected in series with the requirement that steering in one DOF may not be influenced by the rods and hinges for steering in the other DOF. This means that for this mechanism the tip has two rotation points, one for each DOF and the total mechanism becomes complex.

A free connection between transmission elements and the joints can be established via two different approaches, rods placed above joints and rods placed between joints. Rods placed above joints transfer motion and forces via friction or a geared connection.

Connection via friction is established by creating sufficient friction between the transmission elements and the joints. This friction can be created by placing the rod above the joint and pushing the rod onto the joint. A careful selection of materials and sufficient normal force between the connecting elements enables the mechanism to be both stiff and steerable.

A geared connection provides a shape lock between transmission elements and joints. Applying a geared connection for steering in one DOF implies a gear profile on the transmission element and joint. The rod element is placed above the joint and teeth on the rod were pushed into holes in the joint. Application in two DOF requires a special type of profile which enables steering in one DOF while not affecting the position in the other DOF.

A connection consisting of rods placed between joints can be created with rods applied to push to or pull against joints. As rods are placed between joints, the joint should be able to rotate with respect to the rod in all directions for steering. Furthermore the rods are required to move parallel with respect to each other.

Discussion and selection type of connection

The fixed connection consisting of compliant elements requires input to remain steered which must be applied by the surgeon. This results in undesired fatigue of the surgeon during application of the instrument. Due to high forces which will be transferred through the compliant element the bending section of the element should be as thick as possible. However a thicker bending section results in higher input forces and a smaller steering angle without failing as the compliance of materials is limited and the outside of a thick element should allow large deformations for steering. Therefore a tradeoff between high stiffness and low steer-ability versus high steer-ability and low stiffness arises. This connection type was not investigated further due to the constant required steering input and risk of failure at high forces.

Construction of two parallel located series of joints and hinges used in the hinged connection type becomes complex. This is because each DOF has a different rotation point, and transmission in one plane should not be affected by movement in the other plane. Fitting in a $5mm$ instrument results in very thin rods and hinges which makes a stiff steerable mechanism even more complex. Due to the complexity of the hinged structure this connection type is not used.

The connection type in which friction is applied was evaluated thoroughly via a demonstration model. Goal of the model was to examine whether sufficient friction could be generated for steering in two DOF. From the demonstrator was found that for larger angles the mechanism slips. Rods started to bend as forces were applied not directly on the contact point between rod and joint resulting in higher operation forces caused by friction between rod and frame. Furthermore it was difficult to regulate the amount of normal force to prevent slip while minimizing steering force. When applied in a steerable MIS instrument, the required transmission forces will lead to even higher normal forces to acquire sufficient friction. Because of these issues was determined that a friction based connection was not suited to apply in a $5mm$ instrument. A description of the demonstrator and evaluation is described in Appendix A.

In one DOF a geared connection is possible via a gear wheel, however to enable steering in two DOF

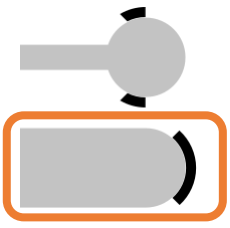

Figure 2.4 – Overview of rod-joint connections. Upper only pull, lower only push.

the toothed profile of both joint and rod becomes very complex as the rod is required to both rotate and steer with respect to the joint. The mechanism could be imagined as a rod with pins attached and a joint with holes comparable to a golf ball. Each of the pins should fit in a hole in the ball. If the ball rotates in the perpendicular plane the orientation of the holes changes with respect to the pins on the rods. Therefore a fit of pin and hole cannot be found for every orientation of the joint. While evaluating the demonstrator described in Appendix A, it was verified whether a profile could be created enabling the two DOF steering motion. Besides when implementing in an $5mm$ instrument the pins and holes become very small and therefore vulnerable for failure.

For the push and pull connection types, displayed in Figure 2.4, achievable thickness of the rods differs when applied to push or pull. As illustrated in the figure a pushing connection allows for a thicker rod. This is due to the characteristic that for a pull connection the rod itself should rotate between the openings of the joint for every steering angle. To enable a larger steering angle of the mechanism, the thickness of the rod reduces. Besides for larger steering angles the opening in the joint increases and the rod is supported only at the outside, as shown in Figure 2.4. This results in a wedging effect between rod and joint inducing high friction forces locking the mechanism. Moreover, as the pull connection is required to be placed in the joint, minimizing to 5mm design leads to challenges as dimensions of rod and joint become very small.

Selected approach

Based on evaluation of transmission elements and connection types was chosen to design a steerable mechanism in which rods will be applied with a push connection with the joints. Using this approach, the stiffness of the transmission elements and joints can be maximized. Rotation in both DOF will be achieved in one rotation point of the joint.

3 Concepts

The objective of the concept phase is to develop design concepts which apply the selected approach of rods used to push to tip and handle joints. First an analysis of the basic mechanism was performed and design challenges were addressed. With obtained knowledge about the mechanism concepts were derived.

Basic mechanism

The basic mechanism which applies rods to push between joints is characterized by three components: frame, transmission elements and joints. A schematic representation of the mechanism was given in Figure 3.1. Black components represent the frame. The frame provides alignment of handle and tip with respect to each other. The frame can as well be applied to support transmission elements. Light grey components represent joints. These components are connected with the frame and are steerable in two DOF. On the tip joint a forceps or needle driver can be attached. The handle joint comprises a joystick to control steering of the tip and a mechanism to open and close the forceps. Dark grey components represent transmission elements, the rods. Rods transfer the forces from the tip to the handle and are only applied to push. Consequently, to steer back and forward in one DOF, two rods are required. To enable steering in both DOFs it was chosen to use four rods in two pairs, each pair controlling one DOF.

For steering, a linear parallel motion was chosen. With the linear parallel motion is meant that the tip joint and the handle joint rotate parallel. As a result of a parallel motion of the tip and handle joints, the mechanism could be made symmetric and therefore the mechanism could be kept simple. To establish the parallel motion of the joints, the joints must be aligned. As a result the forward moving rod and backward moving rod should provide a linear motion while steering. This linear motion of the rods can be provided when the rotation points of the rods and joint are located on the same line. In the schematic presentation in Figure 3.2 this is shown as the rotation points of rods (green dots) and joints (blue dots) always remain on the same line. The upper image shows the position of all rotation points in the mechanism. The lower image shows the steering motion of the mechanism which is equal to the motion of a parallelogram in this example.

To evaluate the steering motion, the connection between the tip joint and rods was evaluated. The connection determines how rotation of the handle joint translates into movement of the rod and rotation of the tip joint. Concepts were designed to enable a

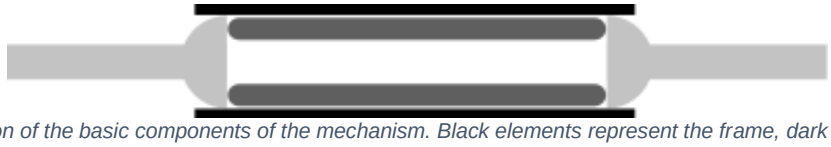

Figure 3.1 – 2D impression of the basic components of the mechanism. Black elements represent the frame, dark grey represent the transmission, light grey represent the joints.

steering angle of 45 degrees to each side in two DOF. This was chosen due to the characteristic that for an angle larger than 45 degrees, shear forces in the rod become larger than axial forces. Consequently, high bending forces arise that result in bending of the transmission elements rather than steering the mechanism.

If the mechanism is designed as shown in Figure 3.1 rods will provide a nonlinear motion. This can be evaluated by a close-up as illustrated in Figure 3.3 which shows that in steered position the backward moving rod has a larger displacement than the forward moving rod. This is due to the property that the contact point of the backward moving rod moves to the outside of the rod surface and the contact point at the forward moving rod moves to the inside of the rod surface. The distance between the rotation point of the tip joint and the contact point of backward moving rod increases whereas the distance between the rotation point of the tip joint and the contact point of the forward moving rod decreases. To exclude this nonlinear movement of the basic mechanism five concepts were derived as shown in Figure 3.4.

Concept Sharp Rod end

The sharp rod end concept was created by designing the rod with a sharp point at the end of the rod. For this concept the contact point on the rod is as well the rotation point of the rod end. While steering, the end point of the rod will slide over the surface of the tip joint, as illustrated in Figure 3.4. This results in the parallel motion of the mechanism as rotation points of the rods and the tip joint is located on the same line. Steering in two DOF requires no adaptations to the mechanism. However if a point contact is used, all forces will lead through that point resulting in high stresses at that point as the area decreases to zero. The sharp end of the rod is therefore likely to deform. Besides deformation, the sharp end will tend to lock in the surface of the tip joint causing the mechanism to lock instead of steer. Appendix B describes a test with the sharp rod ends in which was found that rods lock into the surface of the joints. Due to these issues the sharp rod end concept provided not a viable mechanism and was not developed further.

Concept Holes

The Holes concept is created by fixating the position of rods towards the joints. The working principle is likewise a parallelogram which means that while steering, the rods move towards each other. Therefore the distance between the rods deceases while steering and the moment arm (as displayed in Figure 2.1) of the rod, in the moment equation, decreases. To maintain static equilibrium, forces in the rods must therefore increase.

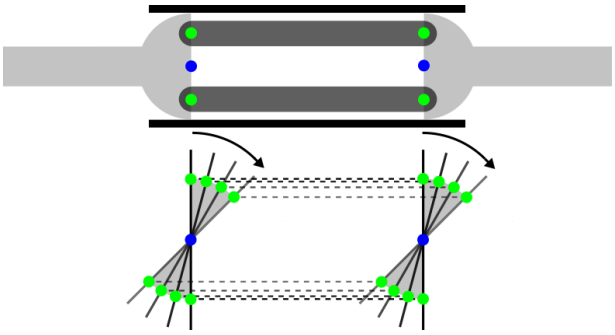

Figure 3.2 - Schematic overview of the parallel motion. The green and blue dots represent the rotation points of the rods and joints. Above shows the location in the mechanism and below shows the motion of steering compared to a parallelogram.

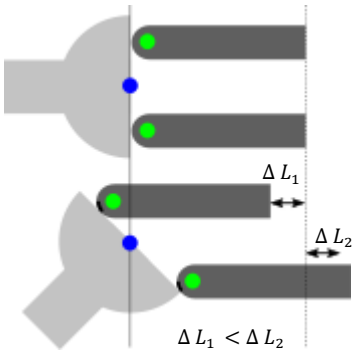

Figure 3.3 - Nonlinear motion rods while steering. The forward moving rod displaces less than the backward moving rod

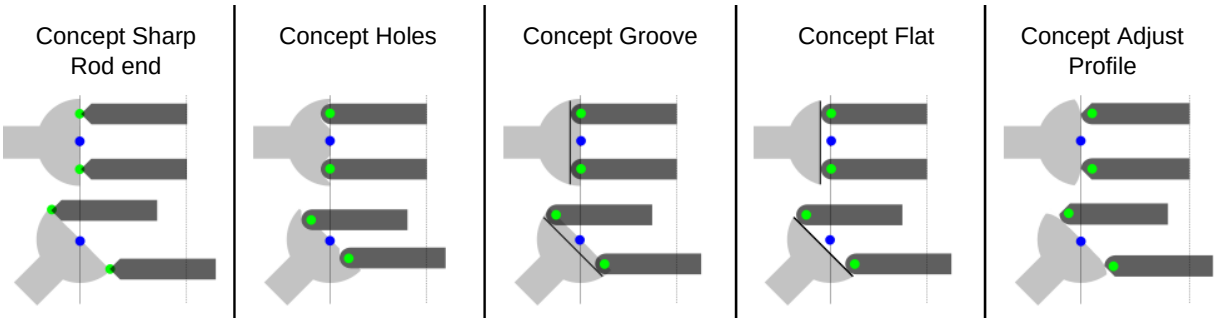

Figure 3.4 - Overview of the five concepts to generate a parallel motion of the mechanism.

To enable parallel motion of the mechanism in 2D, the contact point between rods and joint is required to be placed behind the rotation point of the tip, as displayed in Figure 3.5. To obtain the parallel motion, the radius of the hole is required to be equal to the radius of the end of the rod. As the joint should be able to rotate with respect to the rod, the sides of the hole must be chamfered. The angle of the chamfer in Figure 3.5 is 45 degrees, resulting in a maximal steering angle of 45 degrees to each side. As rods are enclosed by holes in the joint, alignment with respect to each other and the frame is established as well. However, if the steering angle increases above 44 degrees, the rods are no longer enclosed by the frame and are able to fall out of the mechanism as displayed in Figure 3.6. To maintain connection between rod and joint, the steering angle of the mechanism can either be limited to 44 degrees or rods should be supported at steering angles larger than 44 degrees.

To steer in the second DOF, two rods were added placed in the perpendicular plane. While the joint rotates up or downwards, middle rods are not allowed to move. As the rotation points of the rods and joints were placed along one line for every angle, the middle rod will be stationary while moving up or down. An impression of the joint is presented in Figure 3.7.

Concept Groove

Groove concept employs the parallel motion of rods likewise the Holes concept. The major difference is that in this concept the vertical position of the rods, with respect to the frame, is fixed and the position of rods towards joints changes when steering. Therefore rods were required to slide along the joint surface, as can be seen in Figure 3.4. Grooves were chosen to guide the rods in the desired sliding orientation, and therefore prevent bending of the rods in other directions. Also in this concept the rotation points of the rods and joint remain on one line, resulting in the parallel motion. This was provided by choosing the depth of the groove equal to the radius of the rod end. Because the distance of the rods towards the frame is fixed, the moment arm of the rod in the static equilibrium stays equal while steered and is therefore larger than in the Holes concept. However due to the requirement that the rod should always be in contact with the surface of the joint, the maximum achievable steering angle depends on the distance of the rod towards the center of the mechanism. Addition of the second DOF to the mechanism required no further adaptations of the rod or joint as the radius of the end of the rod was already equal to the depth at

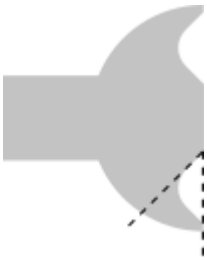

Figure 3.5 - Tip design of rod in hole concept.

Figure 3.6 - Rods no longer enclosed by the hole if the steering angle is equal of larger than 45 degree.

which the surface was placed behind the rotation point of the joint. The resulting surface of the joint is displayed in Figure 3.8.

As rods are supported, the mechanism is in theory suitable to enable steering angles larger than 45 degrees without adaptions besides locating the rods more to the center of the mechanism. However evaluation of the forces on the rod show that for angles larger than 45 degrees, shear forces on the rod become larger than axial forces.

Concept Flat

The Flat concept applies the same working principle as the Groove concept. In this concept no grooves were created as the surface of the joint was made flat at a depth behind the rotation point of the joint equal to the radius of the rod, shown in Figure 3.9. Therefore this concept enables the application of multiple rods, as the rods were not required to slide through a groove in the joint.

Concept Adjust Profile

The Adjust Profile concept was initiated to improve the previous concepts in which the rods touch the joint behind the rotation point of the joint. As the thickness of the joint is limited by the instrument dimensions, it makes the joints weaker. Therefore this concept aims to adjust the joint surface such that the linear parallel motion of the mechanism is possible without the requirement that rotation points of the rods and joint are on one line. Rods touch the joint along the centerline as can be seen in Figure 3.4.

This was achieved by adjusting the mechanism shown in Figure 3.3. The distance of the rod towards the center of the mechanism was chosen that the forward moving rod always slides over a different

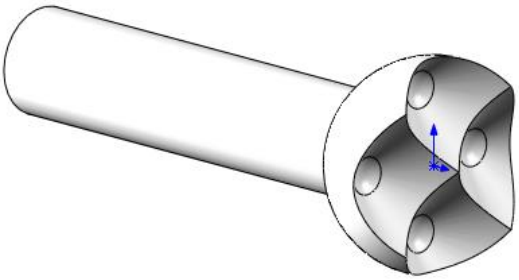

Figure 3.7 - Impression of the Holes concept joint.

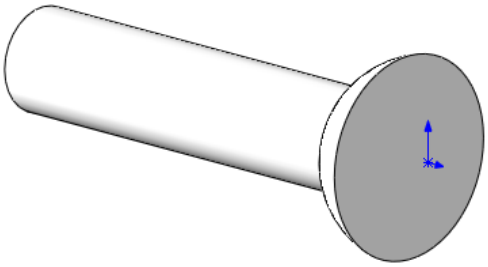

Figure 3.9 - Impression of the Flat concept joint.

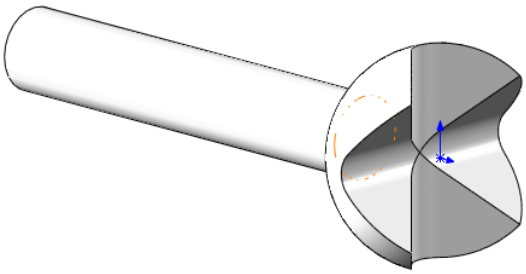

Figure 3.8 - Impression of the Groove concept joint.

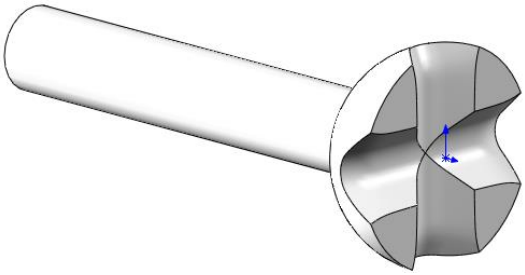

Figure 3.10 - Impression of the Adjust Profile concept joint.

part of the joint surface than the backward moving rod. The assumption was made that the contact point between the backward moving rod and the joint is always located at the center of the rod's end. Adjustment of the outside of the joint surface results in a linear motion of the rods.

The adjusted part of the joint profile in 2D was derived according to the following reasoning:

From the mechanism the height of the rod y_{rod} and the radius of the end of the rod r_{rod} is known. An overview of these dimensions can be found in Figure 3.11.

First the x position of the rod with the sharp end is determined as can be evaluated from Equation 3.1:

$$x(\varphi) = -(tan(\varphi) \cdot y_{rod}) \quad (3.1)$$

The y position of the contact point between the actual rod and the joint is determined by subtracting the vertical component of the contact point on the surface of the rod from the height of the center of the rod as can be seen in Equation 3.2:

$$y_s(\varphi) = (y_{rod} - sin(\varphi) \cdot r\_rod) \quad (3.2)$$

The difference between the x positon of the sharp rod end and the x position of end point of the actual rod is determined by Equation 3.3:

$$\Delta x(\varphi) = -x(\varphi) + (tan(\varphi) \cdot y_s(\varphi) + (1 - cos(\varphi)) \cdot r_{rod}) \quad (3.3)$$

Using Equations 3.1, 3.2 and 3.3 the x position and the y position of the new adjusted profile is determined in Equations 3.4 and 3.5:

$$x_{profile}(\varphi) = cos(\varphi) \cdot \Delta x(\varphi) \quad (3.4)$$

$$y_{profile}(\varphi) = \frac{y_{rod}}{cos(\varphi)} - \sin(\varphi) \cdot \Delta x(\varphi) \quad (3.5)$$

By adjusting the joint profile and the assumption that the backward moving rod touches the joint surface at the center of the rod, the parallel motion of the mechanism was established. As a result of the assumption, the end of the rod requires an adjusted design. This rod design is shown in Figure 3.12. Forces on the endpoint become high, making this point vulnerable for failure. Moreover the orientation of the rod towards the joint should be fixed, resulting in a specific design of frame and rods.

To add the second DOF, two rods were added similar the other concepts. While the mechanism is steered upwards or downwards, the rods in the middle should not displace. Stationary middle rods were achieved via two solutions, one in which the rods were adjusted and one in which the profile of the joint was adjusted.

Rods were adjusted by creating a sharp edge at the end perpendicular to the profile of the rod. Due to high forces in the rods, the sharp end of the tip will be very fragile especially when only the endpoint of the rod touches the joint.

Adjusting the joint is performed likewise the Groove principle by placing the rod in a groove with a depth equal to the radius of the rod end, is displayed in Figure 3.10. To enable steering in two DOF using the working principle of this concept requires that rods were placed more towards the center of the mechanism. This results in increased forces in the rods because the moment arm of the rod in the static equilibrium decreases.

Concept selection

Each successive concept (Holes, Groove, Flat, Adjust Profile) aimed to improve drawbacks of the previous concept. The Groove concept resolved the challenge of the Holes concept of a diminishing moment arm between rod and joint as rods will move only axially. Moreover, the rods are supported in this concept diminishing the chance of buckling. The Adjust profile concept aimed to resolve the challenge of placing the contact between rod and joint behind the rotation point of the joint. However this concept did not succeed as both rod and joint had to be adjusted and still the contact point was placed behind the rotation point of the joint. This made the Adjust profile more complex compared to the other concepts whereas there were no advantages.

From this evaluation was concluded that the Holes, Groove and Flat concepts will be developed further into proof of concept prototypes as these show the highest potential for creating a robust stiff steerable instrument while minimizing complexity of the mechanism.

4 Proof of concept

Selected concepts were developed further into proof of concept prototypes. The prototype mechanism, shown in Figure 4.1, was designed that only joints had to be replaced in order to evaluate a different prototype. If required, support elements were added for support of rods. Goal of the proof of concept prototypes was to determine whether the concepts behave as expected and generate sufficient stiffness. Furthermore the prototypes were used to evaluate which of the three concepts performs best on steerability and stiffness. In order to enable a good evaluation, the dimensions were scaled by a factor of two larger.

An overview of the prototype is provided in Figure 4.1. Five different elements can be distinguished: frame stand, cardan ring, alignment rod, rod and joint. The length of the mechanism, measured between the rotation points of the joints, was designed to be $100mm$. 2D drawings of all elements of the prototype can be found in Appendix C.

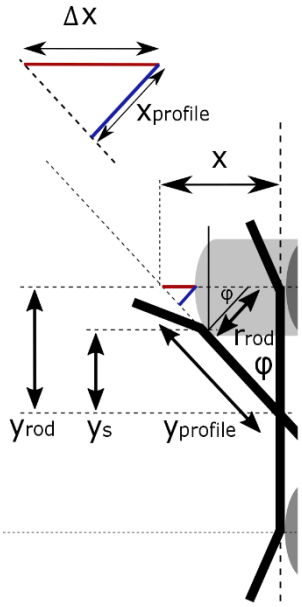

Figure 3.11 - Overview of calculation of the adjusted profile.

Figure 3.12 - Adjusted rod to enable parallel motion via profile.

All elements except the rods, alignment rods and support elements were produced by 3D printing in high detail stainless steel (316L). This manufacturing procedure was chosen as the shape of the joints entailed many small curved details and production via 3D printing was a fast and cost effective alternative to CNC milling.

The used 3D printing technology binds very thin layers of fine stainless steel powder via a precision inkjet printer. After each layer of stainless steel powder a print head moves over the powder depositing a binding agent at designed positions of the constructed part. This layer will be dried by heating and the next layer will be formed on top via the same procedure. After the part was completed it is taken out of all the stainless steel powder that was not bound. The part is then sintered at 1300 degrees Celsius. Afterwards the parts could be polished. [15].

Support elements were 3D printed in the Envisiontec perfactory 4 printer. The used material is EnvisionTEC R5 Gray acrylate. Rods and alignment rods were produced on a CNC lathe machine.

Frame stands were designed robust to prevent that performance of the steering mechanism was influenced by low stiffness of the frame stand. Bottom and side surfaces were made flat to enable good grip while fixating the prototype in a test setup. Four holes were created in which alignment rods

were fitted. The hole in the center was created to guide a threaded rod which was used to adjust the distance between frame stands to eliminate play in the mechanism. The cut-out at the top of the frame stand was made to gain better view on the joint and rod connection while steering. The frame stand has a width of $30mm$, height is $20mm$ and the thickness is $10mm$.

Alignment rods were inserted to prevent torsion. Alignment rods are not fixed within the frame stands to enable adjustment of the distance between the frame stands. Alignment rods have a diameter of $4mm$. The length of the alignment rods was set at $106mm$.

Cardan rings were applied to enable steering of the joints in two DOF. The cardan ring is able to rotate around the horizontal axis with respect to the frame. The joint rotates around the vertical axis with respect to the cardan ring. The cardan ring was designed that the joint was pushed into the cardan ring and the cardan ring was pushed into the frame stand as displayed in Figure 4.2. This enables a quick assembly of different prototypes.

A small pin is placed at the end of the hole to align the joint in the ring as displayed in Figure 4.3. The end of the hole which connects the ring with the frame also contains a pin. The pins were designed to compensate for any inaccuracies in the 3D printed elements. Moreover, the pins will reduce friction between the joint and the ring and between the ring and the frame stand. Cut-outs were made to avoid collisions between the joint and ring and collisions between the rods and ring, which limit the desired steering angle of 45 degrees. The cardan ring was made robust to prevent that it diminishes performance of the prototype. The ring has an outside diameter of $16{,}5mm$ and a thickness of $6mm$.

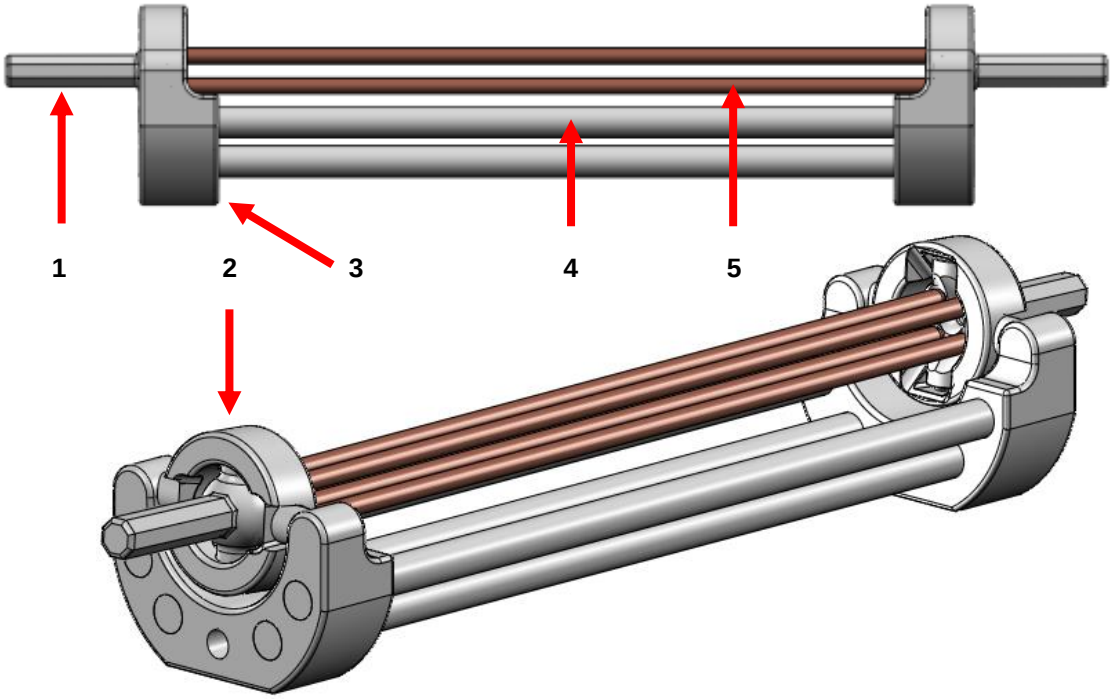

Figure 4.1 - Overview of the proof of concept design: 1) joint, 2) cardan ring, 3) frame stand, 4) alignment rod, 5) rod.

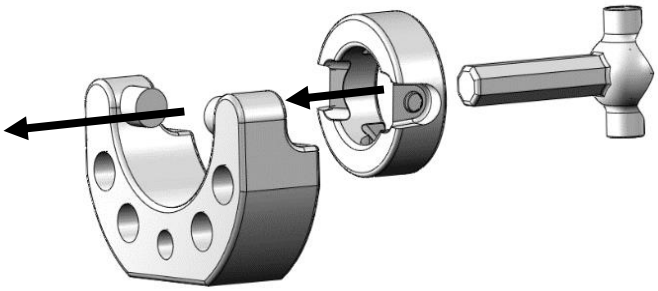

Figure 4.2 - Assembly of the joint in the cardan ring in the frame stand.

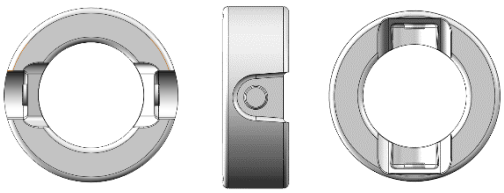

Figure 4.3 - Impression of the cardan ring showing the pins to align the ring in the frame (left and middle image) and to align the joint in the ring (right image)

Rods and joints were designed to enable scaling to 5mm instrument dimensions. To obtain a well substantiated design first the factors that influence stiffness were investigated. Factors influencing stiffness include the amount of rods, rod thickness, radius at the rod-end and position of the rod with respect to the center of the mechanism.

To reduce the amount of force in the rods, the moment arm of the rod should be maximized. Because the outer diameter is fixed, a thicker rod results in a smaller moment arm of the rod. The radius at the end of the rod determines how deep rods will be placed behind the rotation point of the joint. However a bigger radius means that stresses at the rod end will be lower, the joint becomes weaker as the dimensions of the joint are limited to fit in the instrument. Based on these considerations, the rods were chosen to have a diameter of $2mm$ in the prototype design. Rods have total length of $102mm$ and both ends have a spherical shape with a radius of $1mm$. The same rods were applied in all proof of concept prototypes.

All joint prototypes have several common characteristics. The outer radius of the spherical part of the joint is $8mm$. Pins were attached on the top and bottom of the joint to connect the joint with the cardan ring. Radius of the pins is $2mm$ making them strong and prevents bending of the pins, which influences performance of the steering mechanism itself. In the center a hole was created through which a cable can be guided for actuation of the tip. The radius of the entrance is maximized to $2{,}5mm$ enabling fluent bending of the cable. To ease testing, the tip at the back of the joint has an octagon shape. Length of the tip to the rotation point of the joint was set at $20mm$. Characteristics which differ for all prototypes were described in the following sections.

Holes joint

Design of the joint displayed in Figure 4.4 is based on the Holes concept. Characteristic for this joint type are the holes created in the surface of the joint.

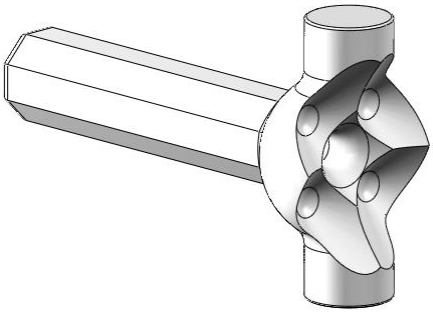

Figure 4.4 -Impression of Holes joint.

These holes have a radius of $1mm$ and the origin of the holes lay at the centerline of the joint. Till an angle a 45 degrees the hole is spherical continuing with a chamfer of 45 degrees outwards. The chamfer enables a steering angle of 45 degrees in all directions, as displayed in Figure 4.4. The center of each hole was placed $2{,}7mm$ from the center of the joints. This distance was chosen because for a larger distance the material surrounding the rod becomes very small and weak. Holes were oriented with an angle of 45 degrees towards the vertical axis in order to achieve maximal support of the pin located at top and bottom.

Expected stiffness and failure modes

As rods were enclosed by joints and high forces were exerted on the rods it was expected that stiffness of the rods is determined by buckling. An evaluation of the static equilibrium displayed in Figure 4.5 showed that rods were enclosed in the joint and therefore axial forces were applied on the rod. The critical axial force can be determined by Equation 4.1:

$$P_{cr} = \frac{\pi^2 \cdot E \cdot I}{(K \cdot L)^2} \qquad (4.1)$$

In which E is the modulus of elasticity of the rod. I is the least moment of inertia. K is the effective length factor which is specific for different connections types of the rod. As the rod is enclosed at both ends, $K = 1$. If the rod is free at one end and fixed at the other end $K = 2$. [10] The length L is the unsupported length of the rod. The critical stress can be determined by Equation 4.2:

$$\sigma_{cr} = \frac{\pi^2 \cdot E}{(L/r)^2} \qquad (4.2)$$

In which E is the modulus of elasticity of the rod. Again L is the unsupported length of the rod. Radius r is the smallest radius of the rod.

If this critical stress is below the yield stress, the rod will deform only elastically. For the proof of concept

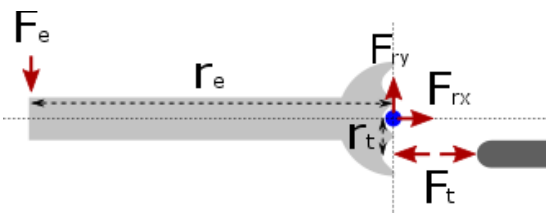

Figure 4.5 - Force evaluation Holes concept as the mechanism is symmetric the side is not displayed.

prototype was calculated that for an axial force of $139N$ rods start buckling. This results in a maximal torque of $375Nmm$ at the tip. Calculation was based on the worst case scenario in which only one rod transfers all forces. If two rods were applied, dividing the force, a maximal torque of $530Nmm$ can be applied to the tip before buckling. Critical stresses for buckling were calculated to be $178MPa$. This is below the critical stress of the 3D printed stainless steel (316L).

Keep in mind that the calculated critical force is the theoretical critical force for buckling. Due to imperfections of the rod and applied force, buckling will probably start at a lower force. Therefore a safety margins should be applied concerning the maximal achievable torque applied to the mechanism.

Groove joint

Design of the joint is based on the Groove concept. The joint contains two grooves in which rods were placed. Rods slide while steering the joint. Both grooves have a depth of $1mm$ behind the rotation point of the joint and continue with a chamfer of 45 degrees. An impression of this joint is provided in Figure 4.6. To prevent collisions between the highest placed rod and the connection pin, part of the pin is cut out. Applying this joint in the mechanism requires two support elements, shown in Figure 4.7, to guide the rods. The holes of the support element have a radius of $1mm$ and the center hole has a radius of $0{,}5mm$. The distance of the center of the holes towards the joint center is $2{,}5mm$. This value was chosen as the maximal distance to remain contact while steered with 45 degrees is $2.83mm$. A margin was kept to ensure contact between rod and joint.

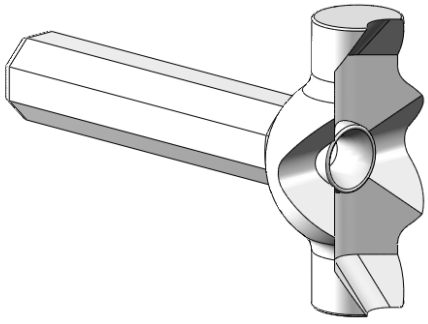

Figure 4.6 - Impression of the groove joint.

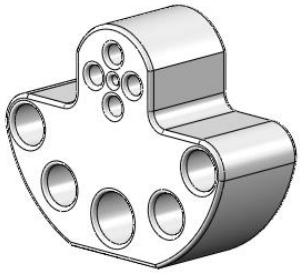

Figure 4.7 - Impression of the support element used in the Groove prototype.

Flat joint

This joint prototype is based on the Flat concept. The prototype contains a flat surface at a distance of $1mm$ behind the rotation point of the joint. An impression of this joint is displayed in Figure 4.8. To support the rods in this prototype, two support elements are implemented. The support elements differ from the one used in the Groove joint as can be evaluated in Figure 4.9. In this prototype the rods are placed with a 45 degree angle towards the vertical axis of the joint to make room for extra supports of the top and bottom pins of the joint, as can be evaluated in Figure 4.8. The transition from spherical part to the top and bottom pin on the joint is made thicker to give more strength to the pin. In a final design these pins could be optimized to create room for a ring of rods steering the joint.

Expected stiffness and failure modes for both the Grooves and Flats.

An evaluation of the forces in the mechanism is displayed in Figure 4.10. Evaluation of the straight orientation shows that axial forces will be applied to the rod. Therefore it was expected that stiffness of the rod was determined by buckling. To calculate the critical load and critical stresses, Equations 4.1 and

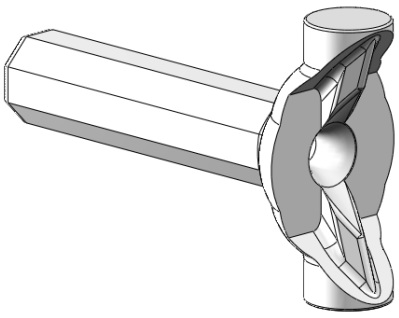

Figure 4.8 - Impression of the Flat joint prototype.

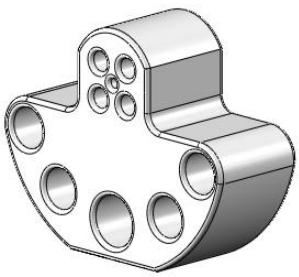

Figure 4.9 - Impression of the support element used in the Flat joint prototype.

4.2 were used. In this case the effective length factor $k = 2$ was chosen as the rod is free to move with respect to the joint. The other side was assumed to be fixed in this static evaluation as it is enclosed by the support element. The unsupported length L was chosen $10mm$. The calculated critical load of the rod for buckling is $3488\ N$. This calculation is based on the worst case scenario in which only one rod withstands all force. As the expected force on the rod is below the critical force the rod is not expected to buckle. If the prototypes were steered the rods touch the joint surface. In this case, besides axial forces also shear forces were applied on the rod and therefore the rod bends. While steered to the maximum angle of 45 degrees, shear forces become equal to the axial forces. If a shear force of $250N$ was applied to the rod, displacement of the rod was determined by the linear beam theory for a beam fixed at one end, shown in Equation 4.3.

$$\delta = \frac{PL^3}{3EI} \qquad (4.3)$$

The free length L was chosen $10mm$. The calculated displacement was $0{,}00059mm$. Based on these calculations was found that the rods, while supported, will experience minimal deformation. It was expected that the sliding joint prototypes in potential provide high stiffness.

Assembly of prototypes

Before assembly of the prototypes, first the elements were inspected. Deviations from the specified dimensions of the elements were addressed and

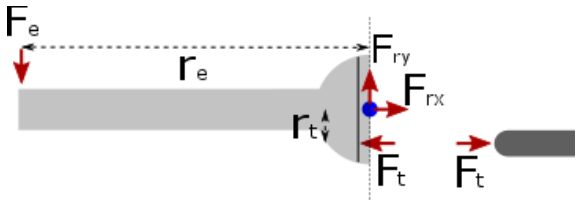

Figure 4.10 - Force analysis groove approach.

elements were prepared to be assembled. Ordered 3D printed stainless steel parts were not polished after production. This was chosen to prevent that any of the details was lost during polishing. An overview of all elements used in the prototypes is shown in Figure 4.11. Additional images of the prototypes and details are displayed in Appendix D

Evaluation of the frame stands showed that the dimensions were equal to the specified dimensions. The pins were polished by hand to create a smooth surface for rotation of the ring. Holes in the frame were drilled to the desired dimensions. Holes in the support elements were also drilled to the desired dimensions.

Evaluation of the cardan ring showed that the distance between the pins which connect with the frame stand was too small. Therefore play was observed between the cardan ring and the frame stand. Probably during sintering the material of the cardan ring deformed towards the center of the ring as this was heated most due to the small thickness. The distance between the pins for connection with the joints was smaller compared to the specified distance. Therefore the joints did not fit within the

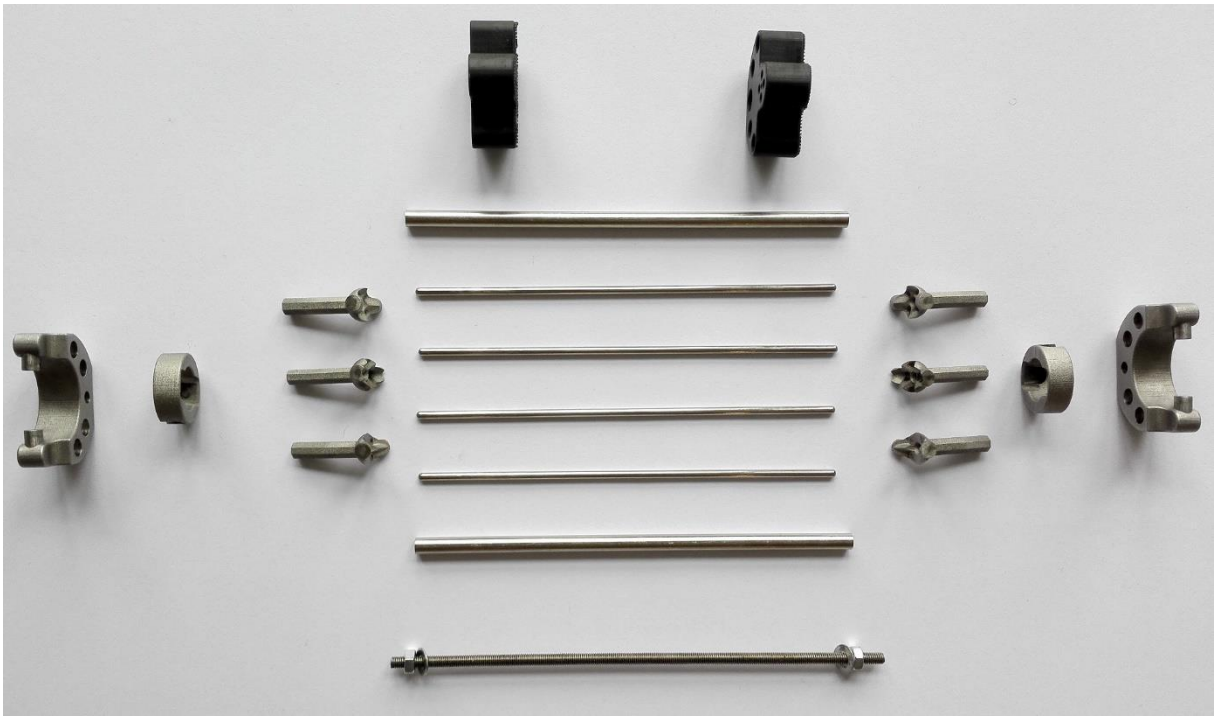

Figure 4.11 - Exploded view of all elemements used to assemble the prototypes.

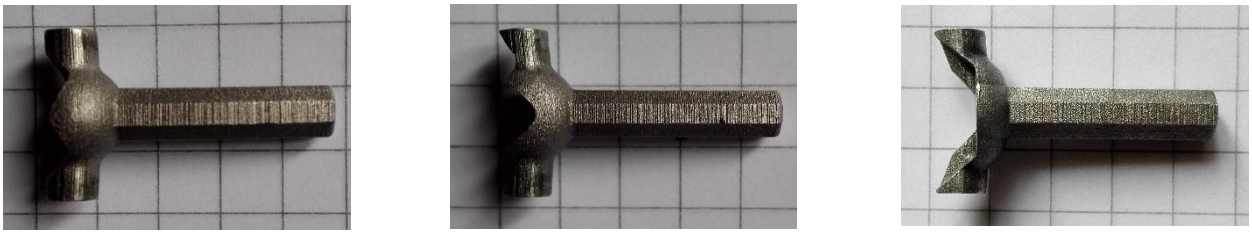

Figure 4.12 - Overview of the joints indicating the bended pins at the top and bottom of the joints.

ring and joints were adjusted to fit. Again this difference with the specified distance could be caused by deformation to the center of the ring during sintering.

Evaluation of the joints show that the pins at the top and bottom were bended towards the profile side of the joint, as displayed in Figure 4.12. Therefore the rotation point of the joint was displaced a little compared to the specified rotation point of the joint. Profiles of the joints seem flat however it was impossible to measure whether the profile is perfect flat as specified. The surface was quite smooth although to create a fluent steering motion of the joints the connections and profile were smoothened by hand. As described, the pins on the joints were adjusted to fit within the cardan ring. For the Flat joint this adjustment resulted in play between the ring and joint as the height of the pin became too short.

5 Testing & results

The prototypes were evaluated using evaluation tests. Goal of the tests was to determine the performance of the prototypes on steer-ability and stiffness.

Test Materials & Methods

An overview of the executed tests is displayed in Figure 5.1. As seen in the figure, three different tests were executed for all prototypes.

Play within the mechanism was evaluated by fixating the handle joint and try to bend the tip joint both in straight orientation and steered. If play was observed in the mechanism causes were analyzed.

Steer-ability of the mechanisms was evaluated by measuring the steering angle of tip and handle in all steering directions.

Stiffness of the mechanisms was verified both in a straight orientation and while steered. In straight orientation force was applied both while one rod withstand force and while two rods withstand the force. While steered the direction in which one rod was required to withstand the force was evaluated.

Used setup for stiffness test

Stiffness tests were performed using a test setup able to measure the applied force and corresponding displacement of the tip. The setup, displayed in Figure 5.2, consists of two sections: one to fixate the frame and handle joint in the desired orientation. The other section contains the force sensor and displacement sensor. This section was used to exert force on the tip by turning the increase force nut. The force-displacement section can be adjusted in height and angle with respect to the instrument fixation section. Used force sensor was a Futek LSB200 (FSH00104) S Beam Load Cell force sensor capable of measuring forces up to $44{,}5N$. Displacement was measured with the Novotechnik TE 50 displacement sensor. Both sensors were attached to a 3016 amplifier; Labjack U3 HV data controller and LJLogUD Logging program: LJControlPanel. The sampling frequency of the logging software was set at $100ms$. The frame of the test setup was made with MakerBeam aluminum beams connected with brackets.

Stiffness evaluation tests were performed according to the following test sequence. First the frame was fixed in the setup. The support elements were placed $5mm$ from the frame stand. Next the handle was steered in the desired direction and angle. The position of the handle was fixed with respect to the

Test	**Orientation**
Play in mechanism	Evaluation of play in straight orientation and while steered
Steering angle	Steering with maximal designed steering angle
Stiffness	Zero degree angle evaluation force applied on one rod
	Zero degree angle evaluation force applied on two rods
	Steered to 25 degrees steering angle

Figure 5.1 - Overview of executed tests for all proof of concept prototypes.

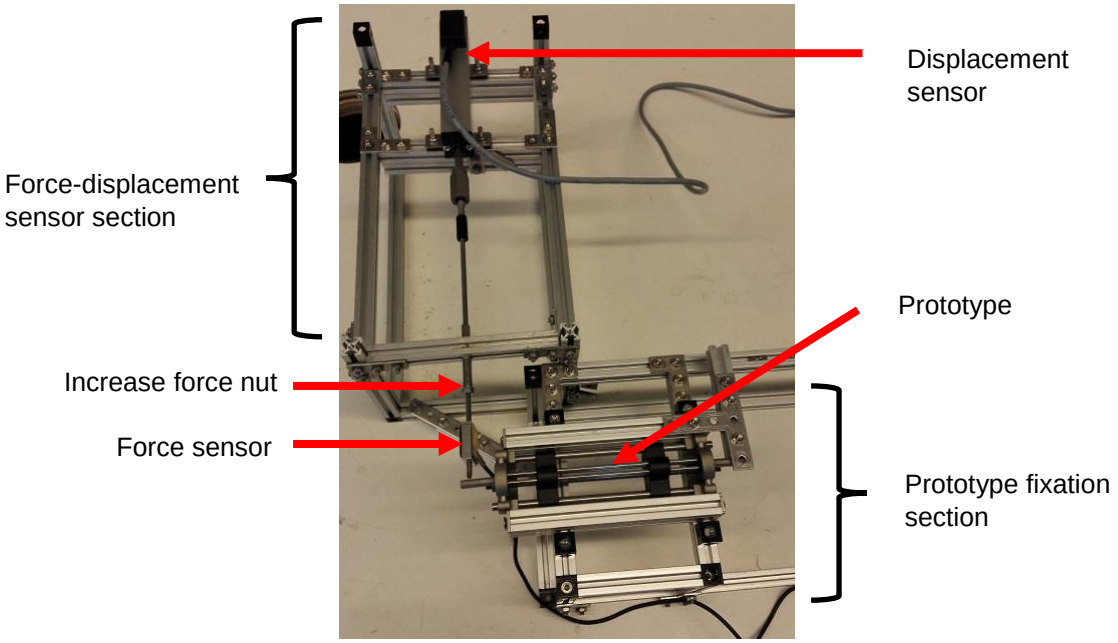

Figure 5.2 - Test setup used for stiffness evaluation tests.

setup. Sensors were aligned perpendicular to the tip joint at a distance of $15mm$ from the rotation point of the tip joint. Before the measurement started a force of $1N$ was applied to the tip joint to diminish play. Gradually force was increased by tightening the force increase nut until a force of $15N$ was reached. Meanwhile both force and displacement were recorded. Each test was performed five times. More details about the used test setup and test results is described in Appendix E

Test results play in mechanism

Evaluation of holes prototype revealed no play in the mechanism for every steering angle. However compliance can be felt when fixating the handle joint and pushing to the tip.

In the Groove prototype play was observed in the horizontal plane while the mechanism was in the straight orientation. In the straight orientation no play was felt in the vertical plane. While steered play was observed both in the horizontal and vertical plane.

The Flat prototype experienced no play in the straight orientation of the tip joint. However while the tip joint was steered, play arises both around the horizontal and vertical plane.

Test results steering angle

Evaluation of the Holes prototype resulted in equal steering behavior in all steering directions. However, as described, the design section the steering angle was limited to max 44 degrees to prevent that the rods fall out of the holes in the joints. Furthermore was observed that steering in all directions went smooth.

Evaluation of the Groove prototype resulted in a steering angle in the horizontal direction of 45 degrees to both sides. Steering in vertical direction resulted in a steering angle of 40 degrees. At 40 degrees one of the rods touches the cardan ring. The prototype was able to steer in all directions however in the directions Northwest, Northeast, Southwest and Southeast extra force was required to steer.

Evaluation of the Flat prototype showed for horizontal steering to the maximal steering angle of 45 degrees that the rods tend to slide off the surface of the joint. Vertical steering was possible to the maximum angle. The mechanism was able to steer in all in-between directions to the designed steering angle of 45 degrees.

Test results stiffness

Based on calculation of the expected behavior of rods was found that the Holes prototype could maximally handle a torque of $375Nmm$ before buckling. This corresponds to a force of $25N$ at a distance of $15mm$. As the prototypes were not tested till breakage, a safety margin was kept. Therefore a force of $15N$ was exerted on the tip joint at a distance of $15mm$ of the rotation point. This corresponds to a torque of $225Nmm$.

To relate the obtained results to a commercial available steerable MIS instrument, the Covidien SILS Clinch was tested as well. The test was performed in the straight orientation of the tip while the tip was locked. A force of $7{,}5N$ was applied at $30mm$ measured from the proximal side of the distal bending section. Results were shown in Figure 5.3.

From the tests a median displacement of $5{,}99mm$ was measured. This refers to a stiffness of $1{,}25\ N/mm$.

According to the results of the first stiffness tests was found that compliancy in the setup influences the results. Measurement results of the initial tests are described in Appendix E. To exclude this compliancy, the setup was evaluated by measuring the displacement of a rigid stainless steel rod with a diameter of $\emptyset\ 4mm$. From calculation using the linear beam theory was found that the rod itself would deform $6{,}88 \cdot 10^{-3}mm$. From this was concluded that the measured displacement is caused by the compliancy of the setup. Both used variants of the setup, shown in Figure 5.4, were tested. Results of the compliance of the setup measurement were displayed in Figure 5.5. From the figure can be observed that for a force of $15N$ the rod displaces about $0{,}21mm$ in the horizontal sensor setup and $0{,}34mm$ in the angled sensor setup.

To create an overview of the performance of the prototypes the results were presented in three figures containing boxplots of the measurements, shown in Figure 5.6. Each figure displays the measured displacements for all prototypes while a force of $15N$ was applied at $15mm$ from the rotation point of the tip joint resulting in a applied torque of $225Nmm$. Results of the measurements, shown in Figure 5.6, were corrected for the compliancy in the setup by subtracting the measured compliancy from the measured displacement.

The results of the Holes prototype across all tests showed that steering of the mechanism does not influence the stiffness of the mechanism. A Significant higher stiffness was observed while two rods were applied to withstand external force instead of one. The maximal steering angle in which the mechanism could be tested was limited to 25 degrees. Overall the Holes prototype has a significant lower stiffness compared to the other two prototypes.

The grooves prototype provided the highest stiffness in all tested orientations. However for this prototype steering resulted in a significant lower bending stiffness.

The Flat prototype showed likewise for the steered test a lower stiffness compared to the tests in straight orientation. Moreover the Flat prototype performed worse compared to the Groove prototype.

For scaling the prototypes to $\emptyset\ 5mm$ dimensions it was assumed that bending of the rods was prevented by the support. In the Holes prototype this was not possible and therefore this prototype was

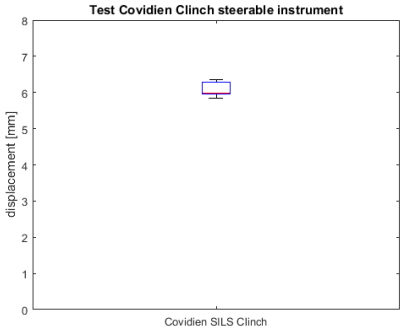

Figure 5.3 - Performance test of the Covidien SILS Clinch instrument. A force of 7,5N was applied 30mm from the proximal side of the bending section.

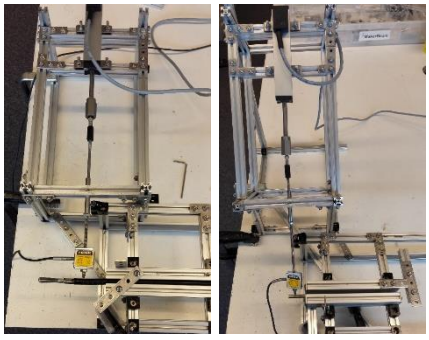

Figure 5.4 - Impression of the used test setup. Left Horizontal and Right angled setup.

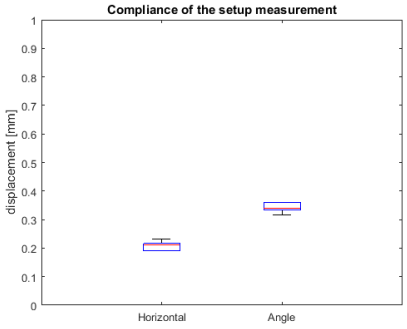

Figure 5.5 - Boxplot displaying the results of compliance measurement of each setup.

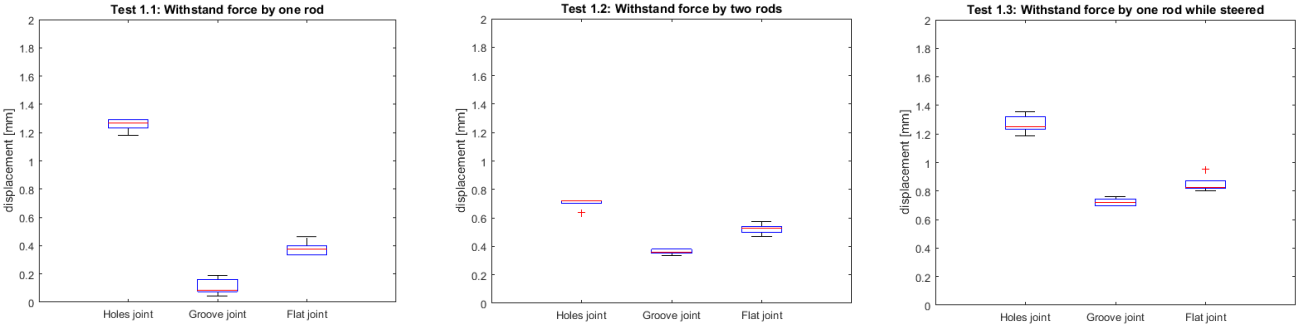

Figure 5.6 - Boxplots showing the deflection of the tip at 15mm from the rotation point while a force of 15N was applied.

not scaled according to $\emptyset\,5mm$ dimensions using this approach. Moreover rods in the scaled Holes Prototype will buckle as calculated by the critical axial load Equation 4.1. Buckling occurs at an axial force of $1{,}05N$. Therefore the rods will already buckle while steering the mechanism. To scale the prototypes, the load displacement Equation (2.1) was applied. For the Groove prototype this results in a stiffness of $3{,}47N/mm$. For the Flat prototype the stiffness becomes $0{,}82N/mm$. A detailed description of the applied method for scaling can be found in Appendix E.

Comparison of the prototypes with the Covidien and the instruments tested by Jelinek et al. is displayed in Figure 5.7 [9]. From this can be found that the Groove prototype possess higher stiffness compared to all other instruments. The Flat prototype provided not an increase in stiffness compared to Covidien and DragonFlex. However in the measured stiffness of both the Groove and Flat prototype the rods were able to bend. Because for scaling was assumed rods will not bend, the scaled stiffness is likely to increase while rods were prevented to bend.

6 Evaluation

Before the most suitable prototype can be chosen to develop further into the $\emptyset\,5mm$ design, the results of the tests were discussed.

Play

Observed play in the Groove prototype in the straight orientation is caused by production of the 3D print as observed by the bended pins at top and bottom. Therefore the vertical groove became less deep compared to the horizontal groove. When assembled rods in the horizontal groove remain free due to this difference in depth of the grooves.

Observed play in the Groove prototype in steered position could be caused as well by production of the joint. During sintering the material further away from the origin will be heated more as thickness decreases. Therefore this is likely to shrink more resulting in a groove which becomes deeper towards the outside of the joint. Based on the characteristic of the principle that rods slide over the surface to the outside of the joint this results in play in the mechanism as can be evaluated by the red profile in Figure 6.1. As both rods experience play, the total play is double the play between one rod and the joint surface. Inaccuracies of the profile further increased play after repeatedly steering the mechanism, causing wear in the grooves. This was found during observation.

	Stiffness [N/mm]
Groove	3,47
Flat	0,82
Covidien	1,25
DragonFlex	2,22
Laparo Angle	0,61
Miflex	0,62

Figure 5.7 - Overview of the comparison between the prototypes and other instruments. From the prototypes the best performing orientation was chosen. For the other instruments the median displacement of the results was chosen to calculate stiffness.

In the Flat prototype the play which was observed when steered could be caused by a surface of the joint which is not perfectly flat caused by the 3D printing production method likewise the Groove joint. Also for this prototype play increased after steering multiple times caused by wear in the mechanism.

For both the Groove and Flat prototypes play was observed between the rods and the support mechanism. Therefore the rods were able to slide over the surface increasing play in the mechanism, especially while steered.

Steering angle

In the Groove prototype the mechanism was able to steer 40 degrees in the vertical direction (upwards and downwards) due to chosen orientation of the rods in this prototype. For this prototype one rod was placed on top, higher than the two rods on top in the other prototypes. However the joint was designed to allow a steering angle of 45 degrees the opening in the cardan ring proved not sufficient to allow a steering angle of 45 degrees.

It was observed in the Flat prototype that due to play in the connection between cardan ring and frame the horizontal alignment of the joint and rods changes, increasing the effect of sliding off the surface.

Stiffness

The steered stiffness test was limited to a steering angle of 25 degrees as for larger steering angles the free rods in the mechanism fell out. Due to buckling

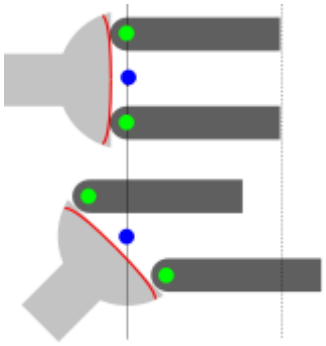

Figure 6.1 - Impression of the influence of a curved surface of the joint.

of the rod which withstands the forces, as observed by the large displacement in the test results, the free rods came loose. In combination with the characteristic of the concept that for large steering angles the rods were hardly enclosed, rods fell out the mechanism. Scaling the Holes concept showed that rods will buckle while steering the scaled prototype. When buckled, the rods will fall out of the mechanism causing the mechanism to fail. Therefore this concept cannot be applied in in a $\emptyset\ 5mm$ dimension design of the instrument.

Comparing the results of the Groove prototype across all tests resulted in a remarkable observation that while one rod was applied the displacement was lower than while two rods were applied. From the size of the box in test 1.1 can be observed that the deviations between the measurements were rather large compared to other tests. Steering results in a much larger displacement of the rod. Further was observed that differences in displacement between the Groove prototype and the Flat prototype were smaller while two rod were applied to withstand force.

Comparing the results of the Flat prototype across all tests also showed that the mechanism performed better while one rod was applied to withstand forces. Further was found that while steered the displacement of the tip doubled, which was a significant difference compared to the straight orientation.

Selection prototype

From the above described results was found that the Groove prototype performs best on stiffness. However was found that a different direction of the applied forces results in a different stiffness of the prototypes. To obtain equal stiffness in all directions a ring of rods should be applied. Moreover a ring of rods distributes applied force over all rods resulting in the least force per rod. Only the Flat prototype is capable of housing a ring of rods. Therefore it was concluded that an improved design of the Flat joint containing a ring of rods which are unable to bend resulted in the most promising mechanism. By selecting a highly precise manufacturing technology the surface could be made flat preventing play in the mechanism while steering.

7 Study 5mm Design

After evaluation of the performance of the prototypes a study was performed to verify whether the mechanism can be scaled down to the dimensions of a $\emptyset\ 5mm$ MIS instrument. In this study, the used principles of the mechanism was kept the same however parts were adjusted to fit in the instrument.

An overview of the design is presented in Figure 7.1, indicating the components of the instrument. Both handle and tip can be steered however the handle cannot close the jaws of the tip.

The shaft consists of a tube with an outer diameter of $\emptyset\ 5mm$ and a wall thickness of $0{,}3mm$. The length of the shaft is $300mm$. At both ends of the shaft a pin is created which supports the cardan ring, displayed in Figure 7.2. The inner surface of the pin has the shape of a hole with a radius equal to the radius of the joint.

The proximal bending and distal bending consist of the cardan ring and joint. As the mechanism is made symmetric only five different type of elements were required to create the steering mechanism: shaft, rod, cardan ring, support element and joint. Zoomed in into the distal bending of the instrument reveals the steering mechanism, as shown in Figure 7.3.

The cardan ring, shown in Figure 7.4, has a spherical shape. This shape was chosen to utilize the available space within the shaft maximally while enabling rotation of the cardan ring in the shaft and rotation of the joint in the cardan ring. The cardan

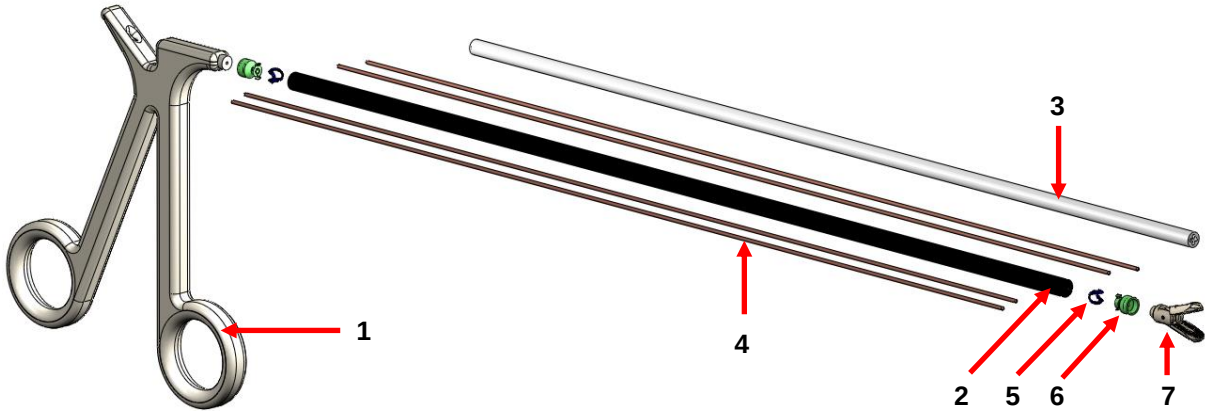

Figure 7.1 - Overview 5mm design Holes concept. 1: handle, 2: shaft, 3: support element, 4 rod, 5 cardan ring, 6: joint, 7: tip.

ring has a thickness of $0{,}4mm$. This was chosen such that the ring is strong enough while maximizing the diameter of the joint. With a larger joint the rods can be placed more to outside and force in the joint can be minimized. Connection between the joint and the shaft was established via holes along the vertical axis and horizontal axis as can be seen in Figure 7.4. At the back a cut out was made to prevent collisions between the rods and the cardan ring while steering as shown in the middle image in Figure 7.4.To create sufficient space for steering the joint with respect to the cardan ring, a cut out was made at the front of the cardan ring shown in the right image in Figure 7.4. A Finite Element Method analysis was performed using Solidworks to evaluate the stress distribution throughout the cardan ring, displayed in Figure 7.5. The cardan ring was locked with respect to the frame and a total force of $250N$ was applied to the connections with the joint. A force of $250N$ was chosen as the worst case scenario in which an external torque of $250Nmm$ is withstand by rods at a distance of $1mm$. From the analysis was found that maximal stresses of approximately $1{,}7GPa$ were found only at the edges of the fillet as can be observed in Figure 7.5. If for example maragingsteel (which is 3D printable) was chosen, stresses remain below the yield stress [16]. However the exact properties of the 3D printed version of this material should be verified by the supplier. Further optimizations of the cardan ring could decrease the stresses further.

Flat joints were scaled to fit within the cardan ring. The pins to connect with the ring were designed with a large radius of $1mm$ to create a large base and prevent deformation of the pin. The joint was evaluated by a FEM analysis in Solidworks. From this analysis was found that stresses in the joint remain below the yield strength if the part is printed in stainless steel 316L. During this analysis the connection pins with the cardan ring were fixed and a force of $50N$ was applied at the end of the joint. The end of the joint was adjusted to fit a handle and tip forceps.

Rods were scaled half the thickness of the proof of concept prototype. As a result, the rods have a diameter of $1mm$. Both ends of the rod have a spherical shape with a radius of $0{,}5mm$. To gain maximal profit of the static equilibrium ratio it is preferable to place the rods as far as possible from the center of the mechanism. A static evaluation of the forces on the rods was performed. From this evaluation was found via calculation of the critical

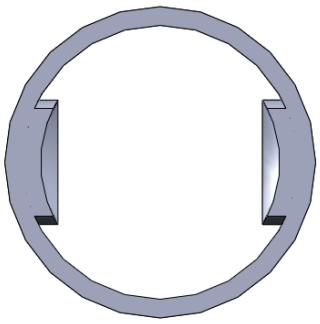

Figure 7.2 - Image of the pins created to support the cardan ring.

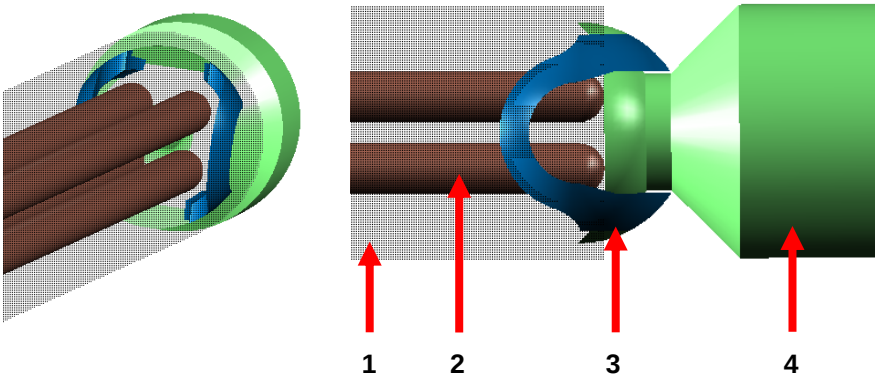

Figure 7.3 - Close up the distal bending. 1: shaft, 2: rods, 3: cardan ring, 4: joint. Proximal bending is equal to the distal bending.

Figure 7.4 - impression of the design of the cardan ring. An overview is shown left. In the middle the top view displaying the cut-out to prevent collision with rods. Right the side view displaying the cut out to enable rotation of the joint

force for buckling that the rods, which are supported, start to buckle at a force of $870N$. For this calculation the equation for the critical force before buckling was applied with a free length L of $10mm$ as the rod is supported by the support element. The effective length factor K was chosen 2 as the rod is free at the endpoint. If an external torque of $250Nmm$ was applied, the force in the rod becomes $250N$ as the rods were placed at $1mm$ distance of the rotation point of the joint. This value is far below the critical force. An evaluation of the axial displacement of the rod showed that a force of $250N$ results in a deformation of $0{,}49mm$ of the rod.

Appendix F shows a detailed description of the $5mm$ design and FEM analysis of the elements.

8 Discussion

In this section the results obtained in this study will be discussed. First the proof of concept prototypes will be discussed followed by the $\emptyset\ 5mm$ design and general remarks.

Proof of concept prototypes

Three prototypes were evaluated: Holes prototype in which rods were enclosed in holes in the joints, the Groove prototype in which rods slide in grooves on the joint surface and Flat prototype in which rods slide over a flat surface of the joints.

Play

The chosen production method of 3D printing in stainless steel resulted in detailed parts. For the frame stands the dimensions were accurate. However because the Groove and Flat prototypes require more accuracy in the joints for good performance this production method proved less suitable. This resulted in play in the mechanism and pins on the joint prototypes which were bended towards the rod-contact surface.

Steering

Steering the Groove prototype in directions between the grooves (northeast, northwest, southeast and southwest) required higher force. This might be caused by the less smooth surface at the sides of the groove. If the joint is then steered for example northwest, the rods are required to both slide in the groove and rotate with respect to the groove. Therefore the rod slides along the side of the groove. This side was not polished as good as the center of the groove.

As the rods in the Groove and Flat prototypes are supported, friction exists between the rods and the

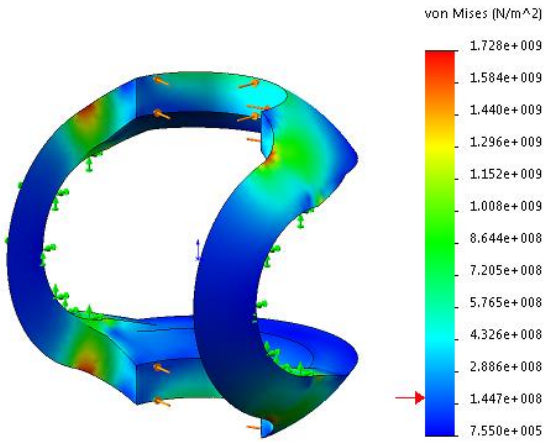

Figure 7.5 - Impression of the FEM analysis of the cardan ring executed in Solidworks.

support elements especially while steered. Moreover as the rods were required to slide over the joint surface this also created friction and both rod and joint surface will wear. Therefore a higher force was needed to steer. Lubrication of all connections will diminish friction and wear, creating smoother and more reliable steering while applied for longer time.

Stiffness

In evaluating stiffness, the measured displacements were corrected with the compliancy of the test setup. This compliancy of the test setup was evaluated by reference measurements with a rigid rod.

After correction, the measurements on the mechanisms showed that stiffness of the Holes prototype is lower compared to stiffness of both Groove and Flat prototypes. This may be caused by the fact that in the Holes prototype the rods were not supported by support elements. As a result the rods will bend. The tests confirmed this as for large steering angles the rods which were not subjected to a force fell out of the mechanism. This can only happen when the rods are bended as the mechanism experienced no play when no external force was applied. Once loaded some rods must be bended to enable enough space for the other rods to disconnect.

The Groove prototype performed best in all tests. Probably this is caused by the characteristic of the prototype that the rods were supported and partly enclosed by the joint. This combines the advantages of the enclosed rods in the Holes prototype with a support added in this prototype.

It was remarkable that both the Groove and Flat prototypes showed a higher stiffness while one rod was required to withstand the $15N$ force. From the

concept point of view no clear cause was found for this behavior of as it was expected that two rods were better able to withstand external forces instead of one. To investigate the cause of this behavior additional tests while the mechanism is steered and tests in which forces are applied from different directions should be performed to exclude influence of the cardan mechanism. An in depth analysis of this behavior is described in Appendix E.

The Flat prototype provided a lower stiffness than the Groove prototype because the rods were able to slide away from the joint surface. However if the rods were made self-supporting with respect to the frame bending of the rods might be prevented. In the prototype this was not introduced to enable an exchange of the joints within the same frame.

In order to reduce costs of the prototypes the same frame was used for evaluation of all prototypes. During tests one setup was available which was adjusted to test different orientations. To enable similar test conditions it was chosen to change the prototype instead of adjusting the setup. This means that for every test the prototype was (dis) assembled again. This could cause small deviations in the performance of the prototypes between different tests.

For scaling the measured stiffness to the $\emptyset\, 5mm$ scale of the mechanism the assumption was made that rods will only deform axially. However during the measurements the rod were able to bend as well resulting in a larger displacement. Therefore the scaled stiffness of the prototypes will be lower than achievable. Preventing bending of the rods will provide even a higher stiffness.

5mm design

As the rods in the mechanisms become very long and thin a support mechanism for rods is required. Otherwise the rods will start to buckle when the mechanism is being steered. Because the rods in the Holes prototype move towards each other it is impossible to design a support mechanism which is able to support every individual rod accurate while enabling independent steering of the joint in both DOF. This can be verified by evaluation of for example the top left rod. If the joint is steered down axial displacement is equal to the axial displacement when steering to right with the same angle. However when the joint is steered down the rod itself must move down whereas when steered to right the rod must move right.

Application of a ring rods results in the lowest achievable force in each rod while applying this type of mechanism. The Flat joint is most suitable for applying a ring of rods, as the surface is flat over the entire joint. Moreover if a ring of rods is applied the mechanism provides equal stiffness for any direction of the applied force. However to the connection pins with the cardan ring should be adjusted to create a round surface of the joint. While a ring of rods is applied the shape of the rods can be adjusted that these cannot bend within the shaft. As a result the stiffness maximizes as rods can only deform axially. Moreover the support element of the rods can be eliminated which eases assembly of the instrument as alignment of the rods with respect to the shaft is provided by the rods themselves.

Limitations to the design

This study focused on the design of the mechanism, however, in clinical use the forceps at the tip will also perform a grasping task. These forces for grasping results in a pulling force which, in the rod design, should be transferred from the tip to the handle via the rods. These additional forces in the rods have not been included in this design and its evaluation.

9 Conclusion

This thesis described the approach, design and evaluation of a new steering mechanism for use in a handheld steerable Minimally Invasive Surgery instrument with high stiffness. From this study the following conclusions were drawn:

As stiffness of the mechanism is determined by the weakest element the most suited approach to create a stiff two DOF steering mechanism with a 5mm diameter is to use solid thick transmission elements that push on joints.

Sliding over a flat surface with a ring of rods results in the best distribution of forces over the rods creating a mechanism with the highest stiffening potential.

Evaluation with a $10mm$ prototype showed a potential high stiffness. Scaling the results to $\emptyset\, 5mm$ dimensions resulted in an at least 2,7 times higher stiffness compared to existing instruments.

FEM analysis showed that the 5mm version can be made robust and it seems plausible that steering capabilities and stiffness maintain. The mechanism meets all requirements which were established at the beginning of this study.

10 Recommendations

Based on the results of this thesis several recommendations for future research were addressed.

For the Flat prototype it is crucial that the surface of the joint is perfectly flat. However from the chosen manufacturing method was found that a small deviation results in play in the mechanism while steered. Other production methods should be investigated to obtain a perfect flat surface of the joints. Furthermore wear of the surface should be prevented.

As the maximal achievable steering angle of the mechanism is determined to be 45 degree in all directions the mechanisms is not suitable for all types of procedures. Therefore an investigation should be performed to determine for which procedures this mechanism is most suited.

This thesis focused on the mechanism for steering. In the final instrument a forceps will be attached to the tip. To enable good actuation the guidance and bending radius of the steering cable should be investigated. For example a Bowden cable could be applied.

An investigation of alternatives for the cardan mechanism can be executed. The goal of this search should be to investigate whether there is a possibility in which the dimensions of the joint can be maximized resulting in a higher stiffness as the rods can be placed further from the center of the mechanism.

The 5mm design of the mechanism could be optimized. Different rod designs can be tested to prevent bending of the rods. Furthermore the joints an ring could be improved to diminish stresses in the elements. Afterwards a demonstration model could be produced to evaluate the mechanism with users.

References

[1] Glasgow, R. E., Adamson, K. A., & Mulvihill, S. J. (2004). The benefits of a dedicated minimally invasive surgery program to academic general surgery practice. Journal of gastrointestinal surgery, 8(7), 869-873.

[2] Velanovich, V. (2000). Laparoscopic vs. Open Surgery. Surg. Endosc., 14(1), pp. 16–21.

[3] Breedveld, P., Sheltes, J. S., & Blom, E. M. (2005). A new, easily miniaturized steerable endoscope. *Engineering in Medicine and Biology Magazine, IEEE*,*24*(6), 40-47.

[4] Bodegom, van R. Creating stiff steerable instruments for Minimally Invasive Surgery: a systematic review (2016).

[5] http://products.covidien.com/pages.aspx?page=ProductDetail&id=195369&cat=Devices&cat2=Model. website visited 10-01-2017

[6] T.G. Cooper, D.T. Wallace, S. Chang, S.C. Anderson, D. Williams and S. Manzo, Surgical tool having positively positionable tendon-actuated multi-disk wrist joint. Intuitive Surgical Inc, US Patent Application Publication 6817974B2, 2004.

[7] Palep, J. H., 2009, "Robotic assisted minimally invasive surgery," *Journal of Minimal Access Surgery, 5(1)*, pp. 1-7

[8] Jelínek, F., Pessers, R., & Breedveld, P. (2013). DragonFlex–smart steerable laparoscopic instrument. *Journal of Medical Devices*, *7*(2), 020911.

[9] Jelínek, F., Gerboni, G., Henselmans, P. W., Pessers, R., & Breedveld, P. (2014). Attaining high bending stiffness by full actuation in steerable minimally invasive surgical instruments. Minimally Invasive Therapy & Allied Technologies, 24(2), 77-85.

[10] Hibbeler, R. C. 2005. Mechanics of materials, 6th ed. New Jersey: Pearson Prentice Hall

[11] Gerboni, G., Henselmans, P. W., Arkenbout, E. A., van Furth, W. R., & Breedveld, P. (2015). HelixFlex: bioinspired maneuverable instrument for skull base surgery. Bioinspiration & biomimetics, 10(6), 066013.

[12] Zhao, R., Zhao, S., & Luo, Y. (2014). Development of a flexible and stiffness changeable mechanism for NOTES. International Journal of Applied Electromagnetics and Mechanics, 45(1-4), 825-831. doi: 10.3233/jae-141912

[13] Yamashita, H., Iimura, A., Aoki, E., Suzuki, T., Nakazawa, T., Kobayashi, E., ... & Dohi, T. (2005). Development of endoscopic forceps manipulator using multi-slider linkage mechanisms. Journal of Japan Society of Computer Aided Surgery, 7(2), 201-4.

[14] Jelínek, F., Arkenbout, E. A., Henselmans, P. W., Pessers, R., & Breedveld, P. (2015). Classification of Joints Used in Steerable Instruments for Minimally Invasive Surgery—A Review of the State of the Art. Journal of Medical Devices, 9(1), 010801.

[15] https://i.materialise.com/3d-printing-materials/high-detail-stainless-steel website visited 08-02-2017

[16] http://www.oceanz.eu/metalen website visited 20-01-2017

Appendix A – Evaluation connection between transmission and joint via friction

The connection between the transmission elements and the joints via friction was evaluated by a demonstrator. Goal of this evaluation was to verify first whether it is possible to steer the joints to large angles minimal 60 degrees in all directions. Furthermore it was aimed to verify whether this mechanism has potential to work on a smaller scale.

To verify this the demonstrator displayed in Figure A1 was build. The mechanism consists of two wooden balls which represent joints. Joints were supported and steered by stainless steel rods placed around the joints. The rods were pressed towards each other by bronze bushings pressed together by a spring. The bushings were supported by frame stands.

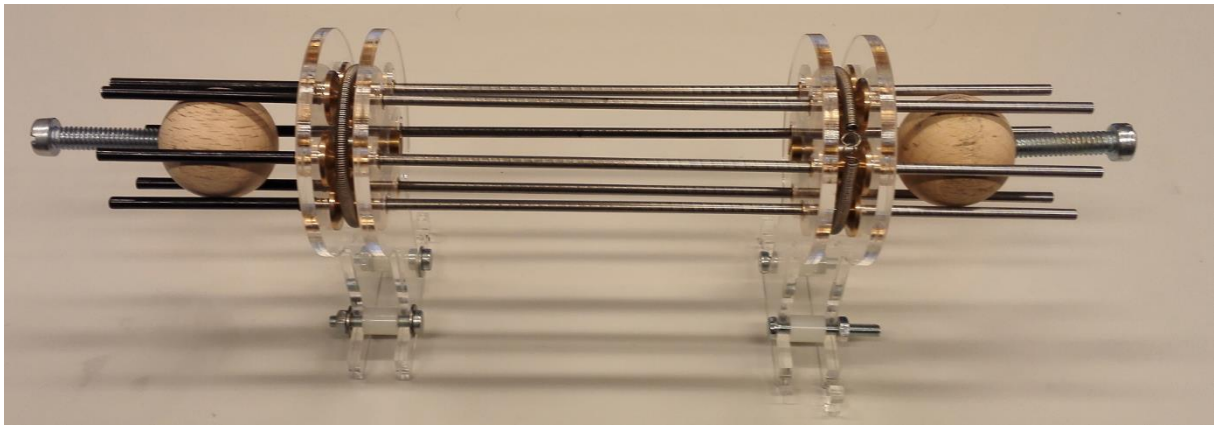

Figure A1- Impression of the friction based demonstrator. Joints were represented by the wooden balls, transmission elements were represented by the stainless steel rods. Springs and bronze bushings were applied to press the rods on the joints.

During evaluation of the demonstrator several issues were observed. Because of the length of the rods the rods started to bend while the spring was attached. Even with a low pretension applied by the spring the rods started to bend. Therefore the rods experienced frictions within the bushings. Already for smaller steering angles the joints start to slip. This was caused partly by the deformation of the rods and the friction coefficients between the wooden balls and the stainless steel rods. To improve stiffness a polyurethane tube around the rod was tested as well. This resulted in a little improved performance.

Based on the observations an estimation was made whether this mechanism is able to be scaled down to 5mm dimensions. It was estimated that because the normal force on the rod and joint results in a delicate balance, the mechanism is likely to lock or slip. Therefore this approach was not chosen to evaluated further.

Appendix B – Evaluation sharp rod end concept

To verify the performance of different steering mechanism a demonstrator was build. The goal of this demonstrator was to evaluate whether the sharp rod end can be applied as a suitable approach for creating a tiff steerable mechanism.

The mechanism, shown in Figure B1, consists of a 3D printed frame section. On each side of the frame a joint was attached. Joints were made from aluminum and stainless steel. Rods with a sharp end were placed between the joints. Joints were supported by screws with an opening to allow rotation of the joint.

Evaluation of the steering motion of the demonstrator showed that the rods tend to lock in the joints instead of

Figure B1 - Overview of the demonstrator to evaluate the performance of the sharp rod end concept

slide along the joint surface. This was observed by the surface of the joints as shown in Figure B2. To prevent this locking of the rods in the joint, a stronger material could be applied however in that case the tip of the rod will wear. Based on this evaluation was found that the Sharp Rod end was not a suitable approach to create a stiff steerable mechanism.

Figure B2 - Impression of the surface of the joint containing wear of the surface due to locking of the rods.

Appendix C – 2D drawings prototypes

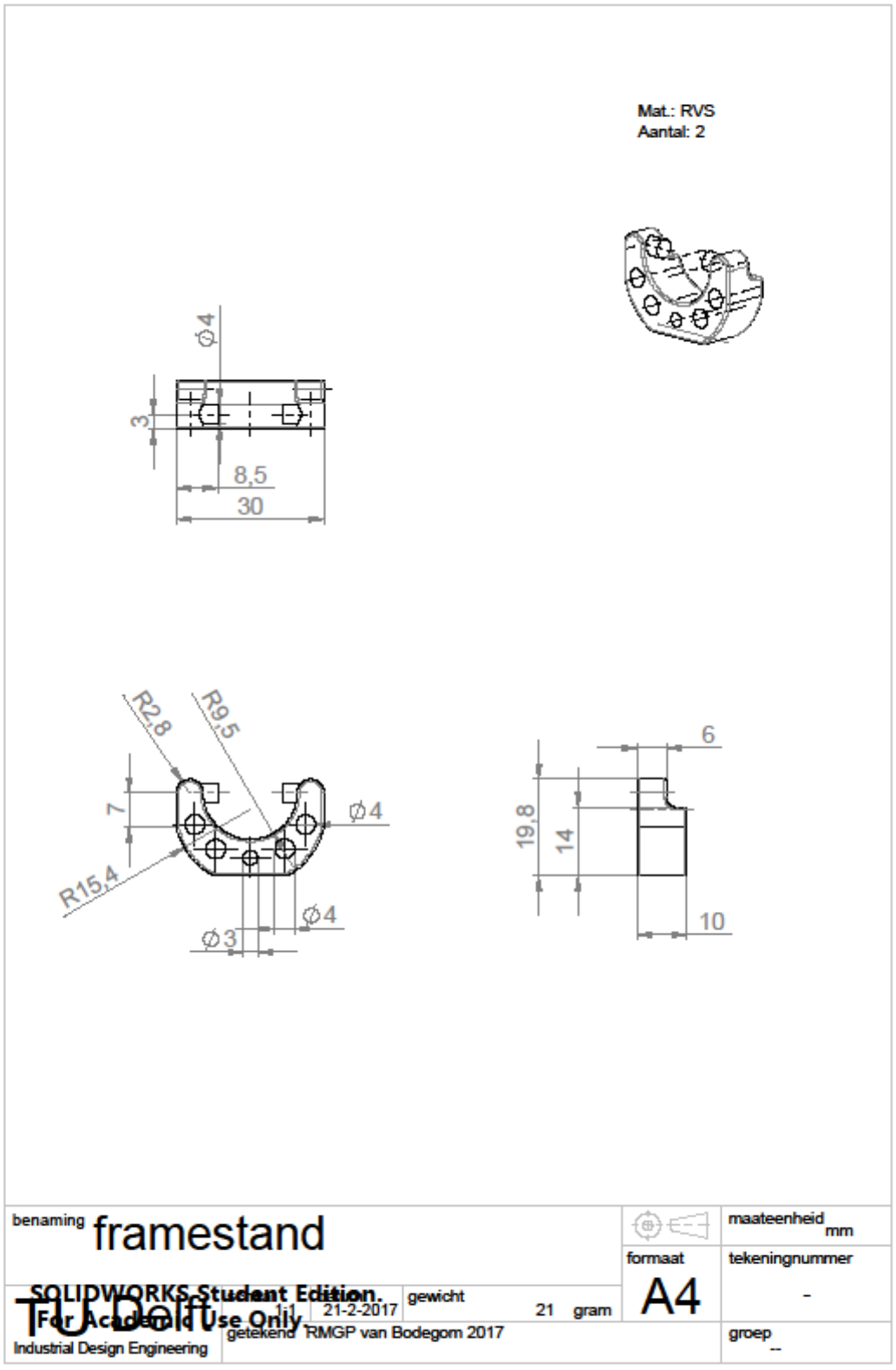

Mat.: RVS
Aantal: 4

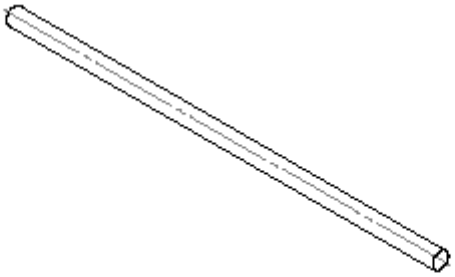

benaming: alignment rod			maateenheid: mm
		formaat: A4	tekeningnummer: -
SOLIDWORKS Student Edition. For Academic Use Only.	schaal: 1:1 / datum: 22-2-2017 / gewicht: 11 gram		
TU Delft Industrial Design Engineering	getekend: RMGP van Bodegom 2017		groep: -

Mat.: RVS
Aantal: 2

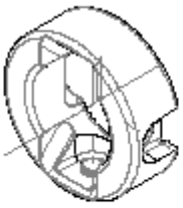

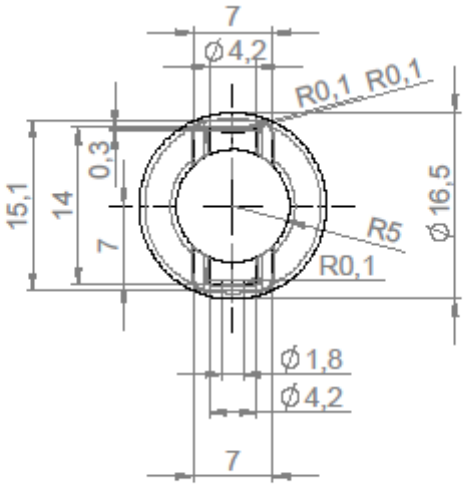

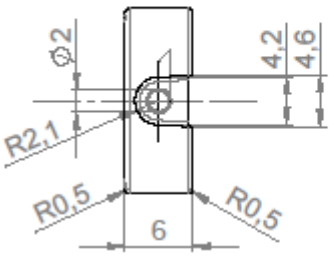

benaming middlering			maateenheid mm
		formaat A4	tekeningnummer -
SOLIDWORKS Student Edition. For Academic Use Only.	schaal 1:1 / datum 21-2-2017	gewicht 5 gram	
TU Delft Industrial Design Engineering	getekend RMGP van Bodegom 2017		groep -

Mat.: RVS
Aantal: 4

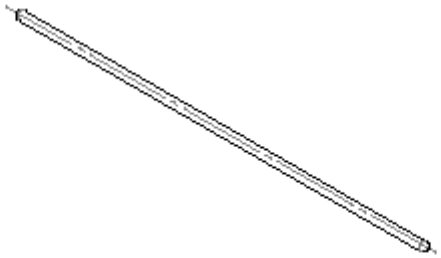

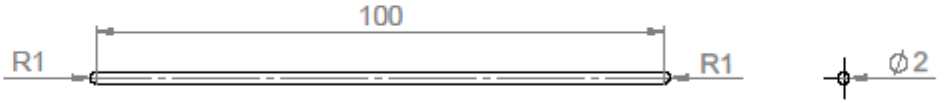

benaming rod			maateenheid mm
		formaat A4	tekeningnummer -
SOLIDWORKS Student Edition. For Academic Use Only.	gewicht 3 gram		
TU Delft Industrial Design Engineering	getekend RMGP van Bodegom 2017		groep -

Mat.: RVS
Aantal: 2

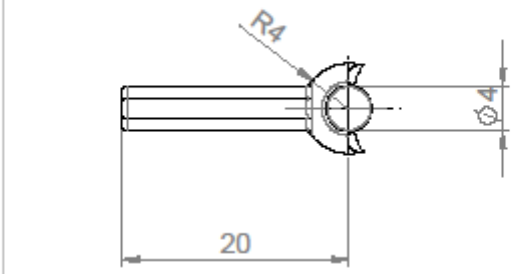

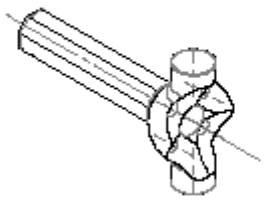

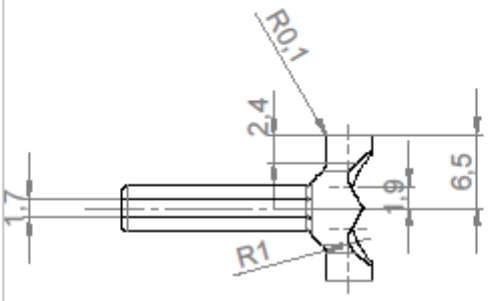

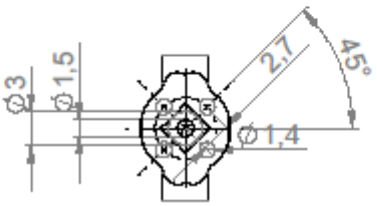

benaming: holes joint			maateenheid: mm
		formaat: A4	tekeningnummer: -
SOLIDWORKS Student Edition. For Academic Use Only.	schaal: 1:1 / datum: 22-2-2017	gewicht: 3 gram	
TU Delft Industrial Design Engineering	getekend: RMGP van Bodegom 2017		groep: -

Mat.: RVS
Aantal: 2

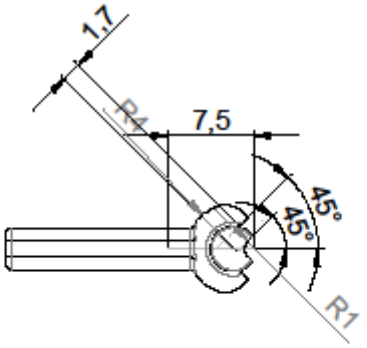

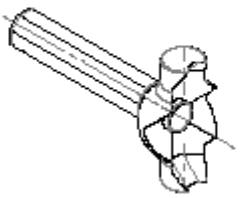

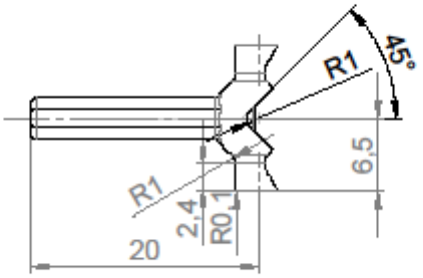

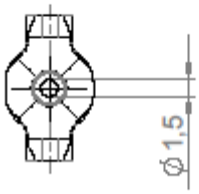

benaming: groove joint			maateenheid: mm
		formaat: A4	tekeningnummer: -
SOLIDWORKS Student Edition. For Academic Use Only	schaal: 1:1 / datum: 22-2-2017	gewicht: 3 gram	
TU Delft Industrial Design Engineering	getekend: RMGP van Bodegom 2017		groep: -

Mat.: Kunststof
Aantal2

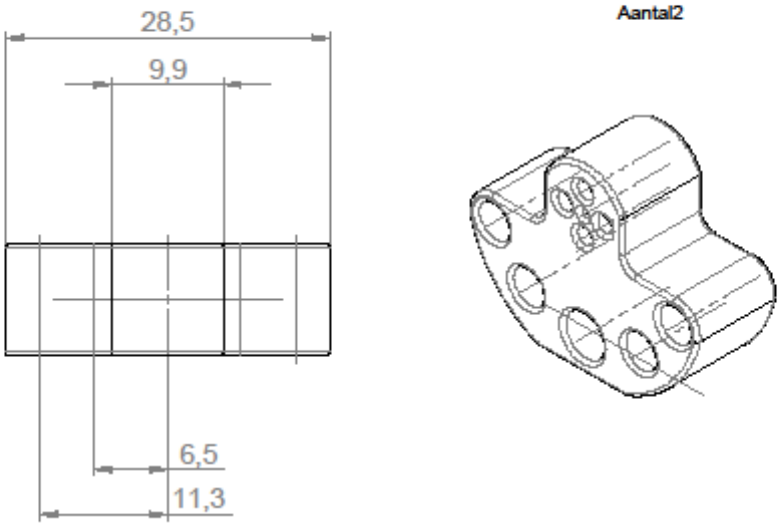

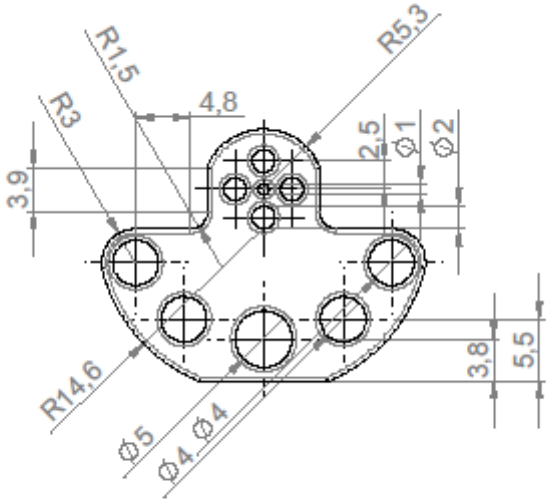

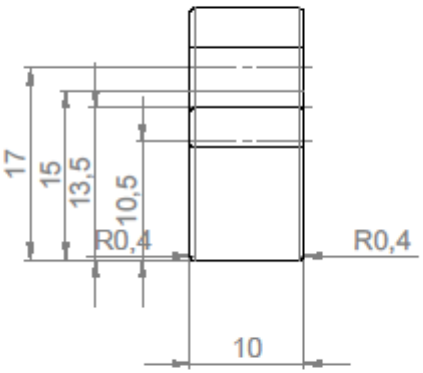

benaming: support groove			maateenheid: mm
		formaat: A4	tekeningnummer: -
SOLIDWORKS Student Edition. For Academic Use Only.	schaal: 1:1 / datum: 22-2-2017	gewicht: 3 gram	
TU Delft Industrial Design Engineering	getekend: RMGP van Bodegom 2017		groep: -

Mat.: RVS
Aantal:2

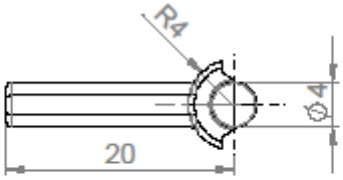

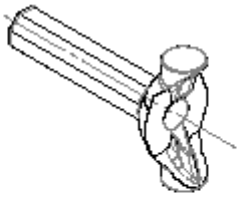

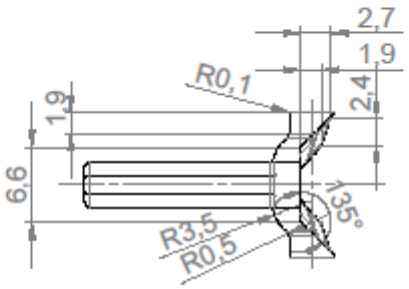

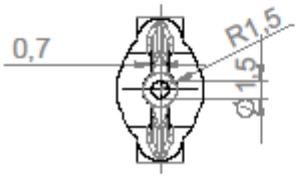

benaming: flat joint			maateenheid: mm
		formaat: A4	tekeningnummer: -
TU Delft Industrial Design Engineering	datum: 22-2-2017	gewicht: 3 gram	
	getekend: RMGP van Bodegom		groep: -

Mat.: Kunststof
Aantal:2

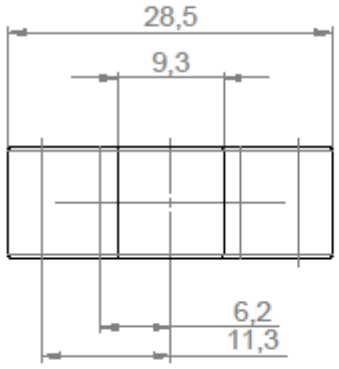

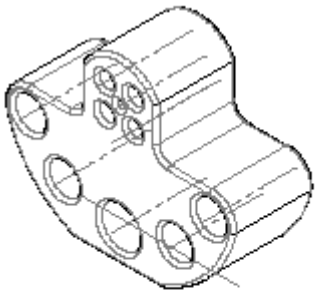

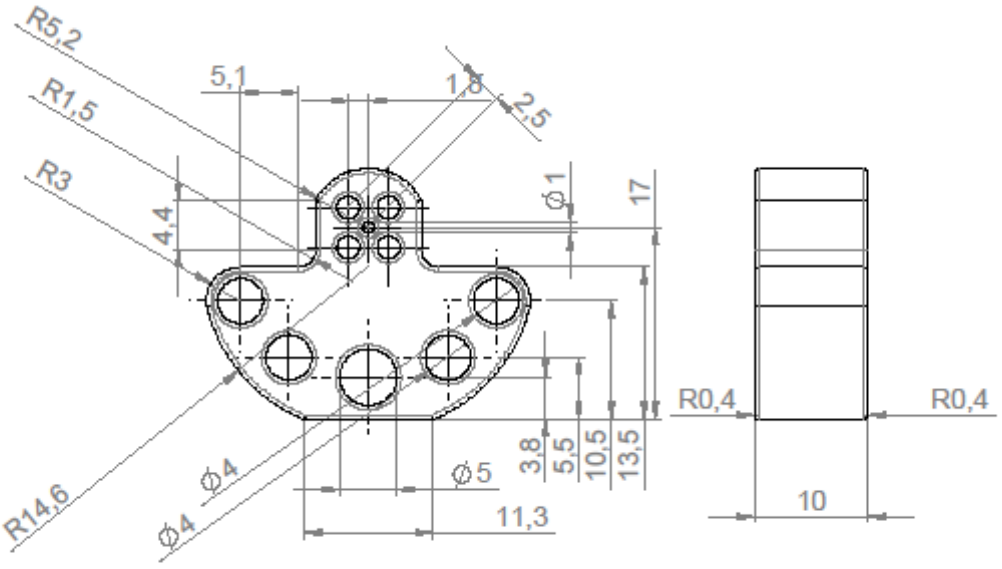

benaming: support flat			maateenheid: mm
			formaat: A4
SOLIDWORKS Student Edition. For Academic Use Only.	schaal: 1:1	gewicht: 3 gram	tekeningnummer: -
TU Delft Industrial Design Engineering	getekend: RMGP van Bodegom 2017	22-2-2017	groep: -

Appendix D – Images prototypes

This appendix shows a series of images from the prototype mechanism.

Appendix E – Prototype evaluation

Images during tests

During the tests several images were made showing the setup and clamping of the prototype in the setup. These images can be found below.

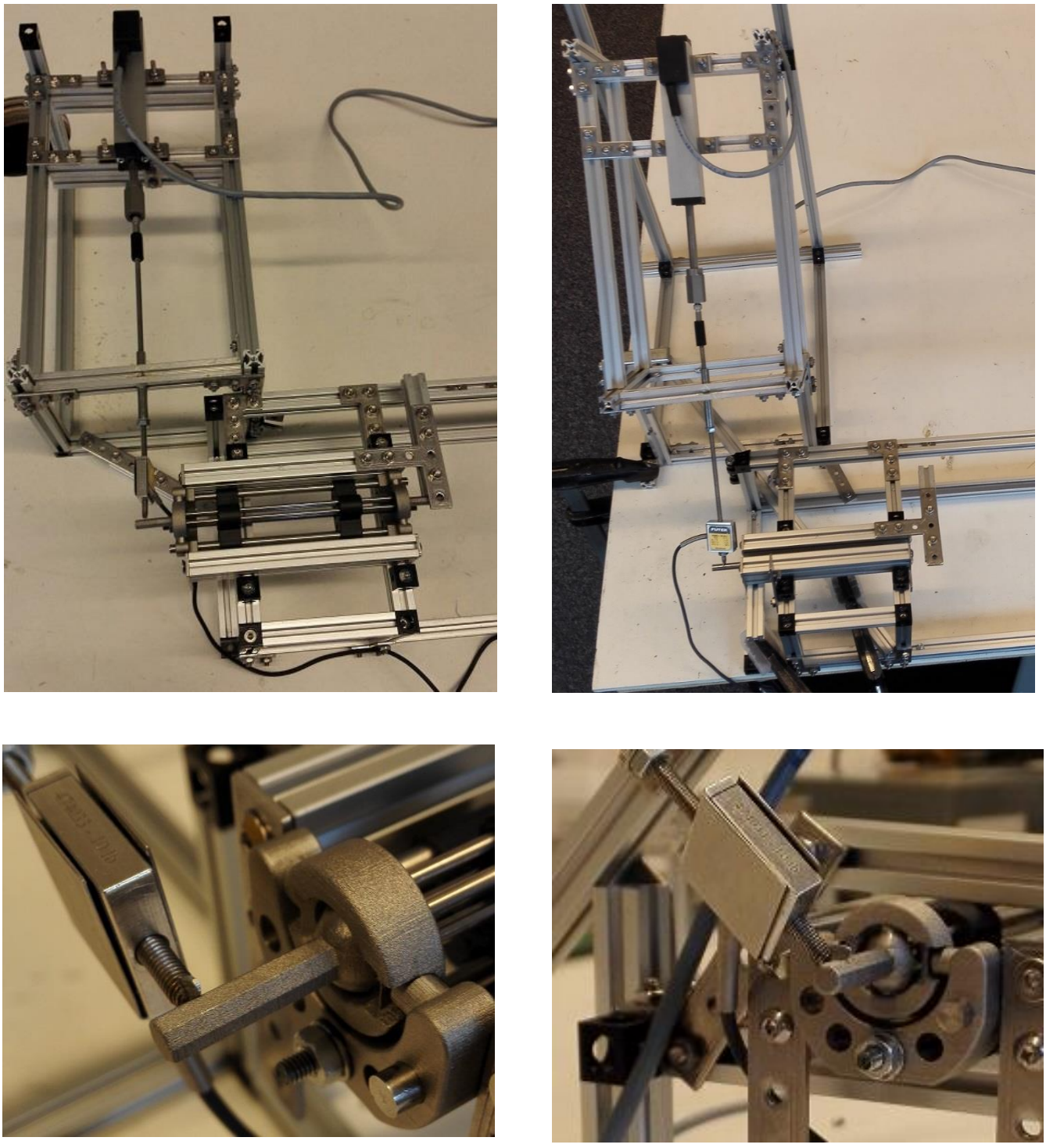

Figure E1 - Images of the two variants of the used test setup. Left the horizontal orientated setup and right the angled setup.

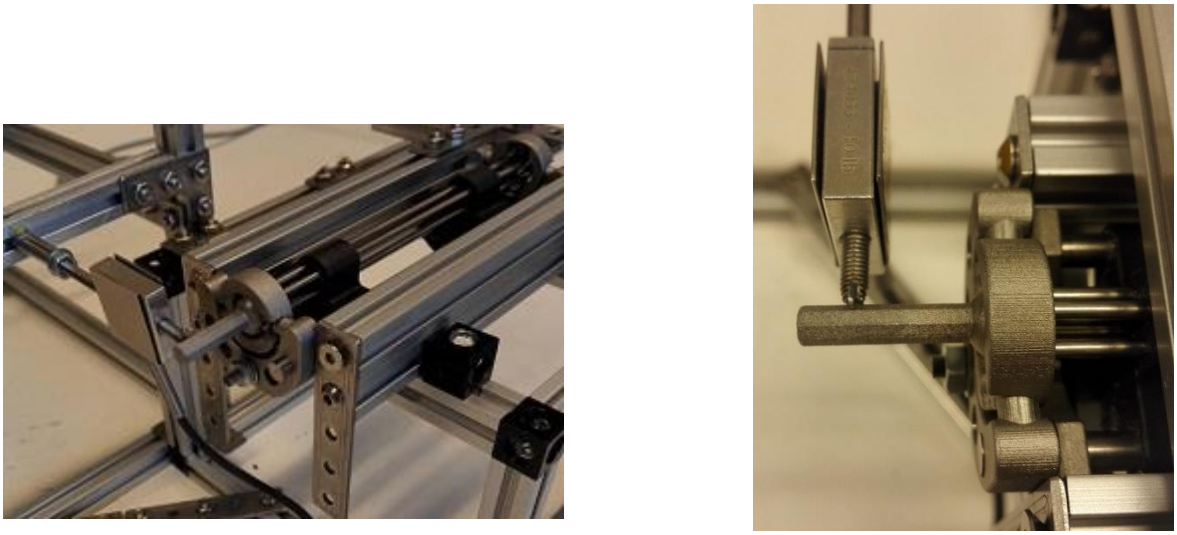

Figure E2 - Impression of the prototype in the setup. Left the entire prototype in the setup and right a close-up of the force sensor touching the joint.

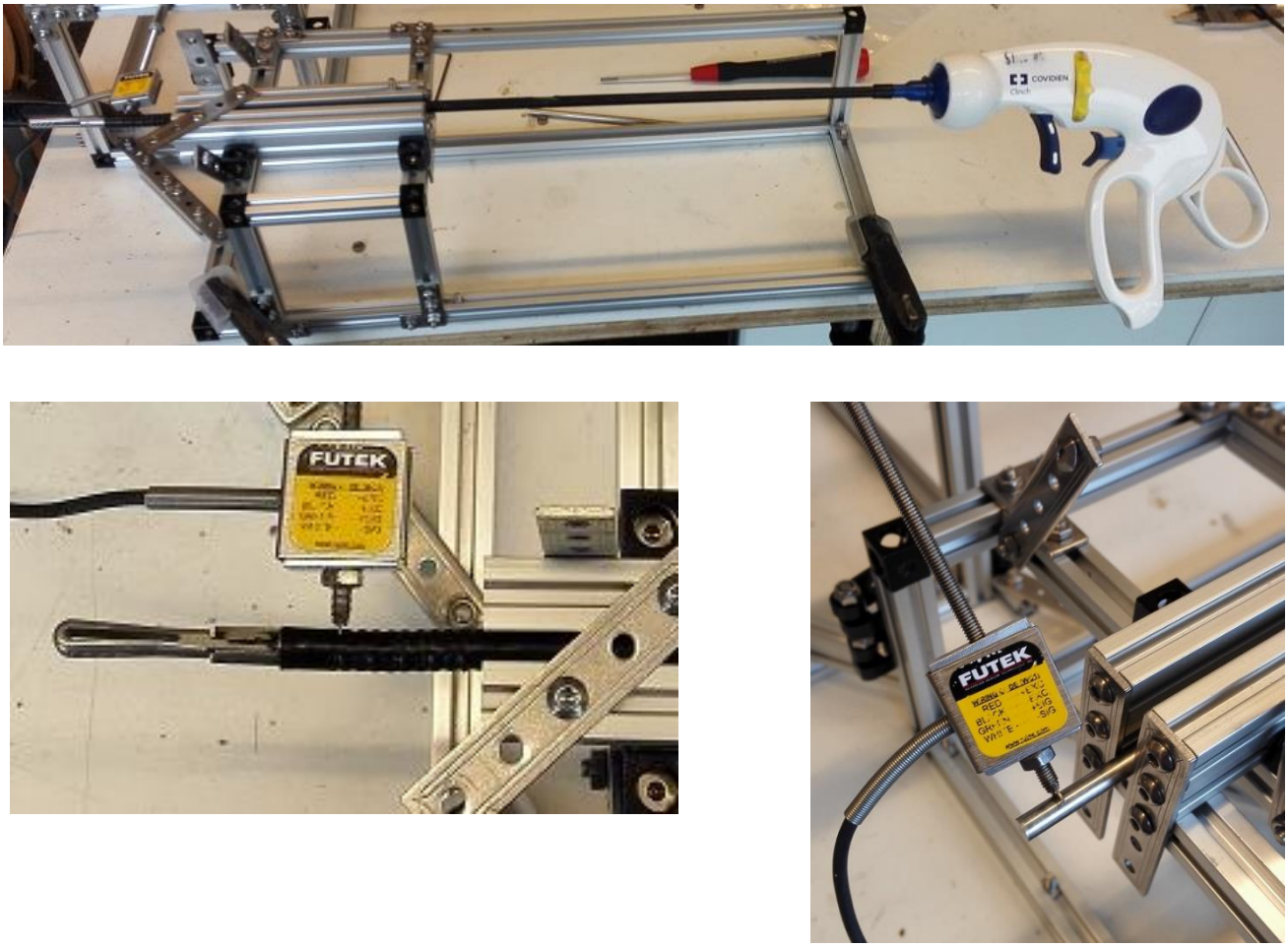

Figure E.3 - Impression of the covidien instrument tested in the setup (above), left a close-up of the force sensor touching the tip. Right shows the reference measurement in which the compliancy of the setup was evaluated. In this case the angled setup.

Test results

Below the figures containing the results of the initial measurements and a table with the measured displacements are provided.

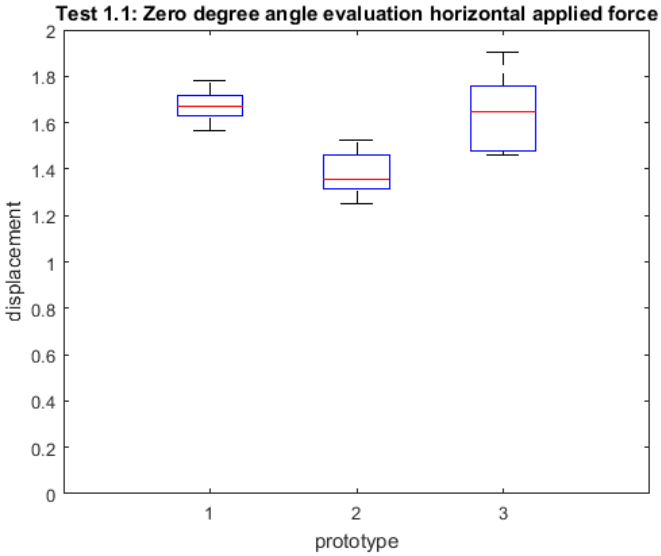

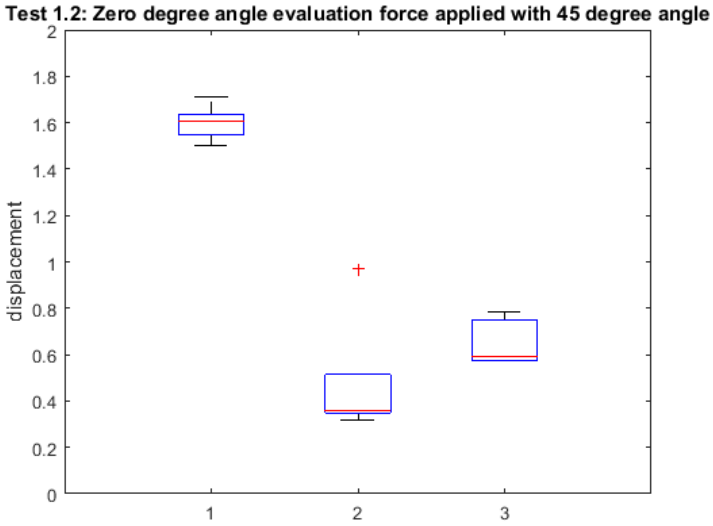

Test 1.1					
Prototype	Measured displacement [mm]				
Holes	1,78	1,65	1,57	1,69	1,67
Groove	1,52	1,34	1,44	1,35	1,25
Flat	1,90	1,49	1,46	1,65	1,71
Test 1.2					
Holes	1,61	1,50	1,57	1,61	1,71
Groove	0,97	0,36	0,36	0,36	0,32
Flat	0,74	0,78	0,57	0,57	0,59
Test 1.3					
Holes	0,59	0,68	0,66	0,68	0,61
Groove	0,68	0,51	0,57	0,55	0,46
Flat	1,27	1,27	1,21	1,08	1,29

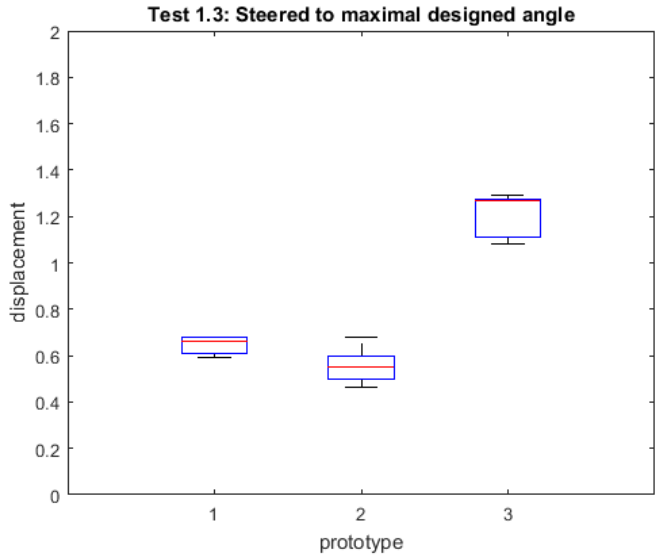

Based on the large size of the boxes in the boxplots was found that the results of the measurement were not very precise. Furthermore was observed during the tests that compliancy influences the measurement. Therefore additional tests were performed. Shown in the images and table below.

Test 1.1					
Prototype	Measured displacement [mm]				
Holes	1,37	1,29	1,50	1,52	1,46
Groove	0,63	0,70	0,68	0,66	0,68
Flat	0,68	0,66	0,59	0,57	0,53
Test 1.2					
Holes	1,61	1,50	1,57	1,61	1,71
Groove	0,57	0,55	0,59	0,57	0,57
Flat	0,91	0,97	0,91	0,87	0,87
Reference					
	0,44	0,40	0,40	0,40	0,42

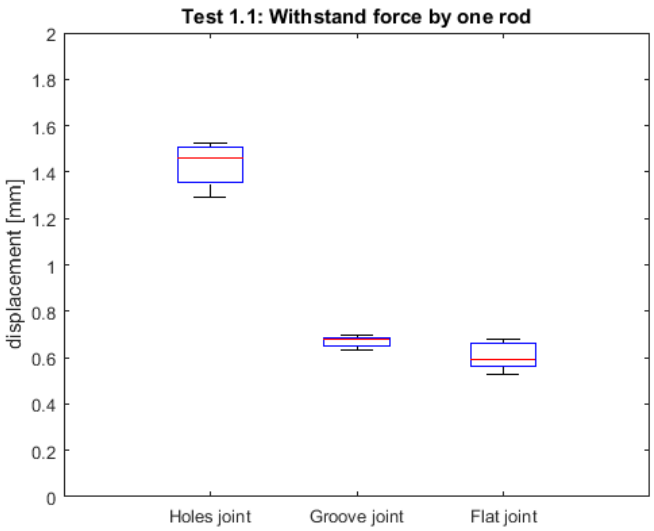

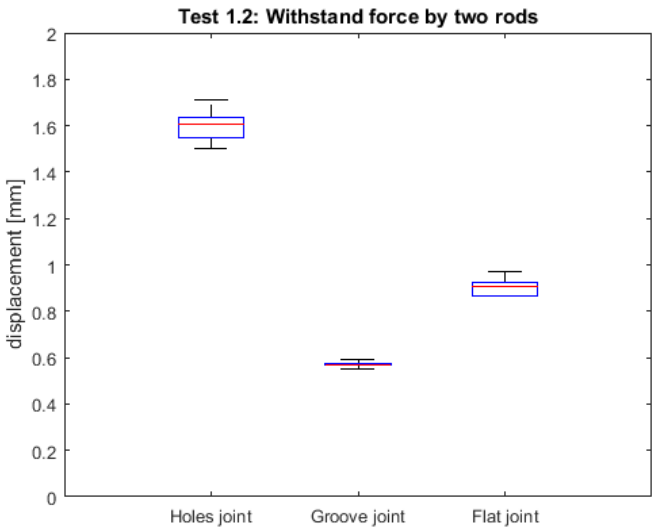

As can be seen from the Figures the results were more precise. However unfortunately compliancy of the setup was evaluated only evaluated for the horizontal orientated force section. In order to exclude all inaccuracies for all tests additional tests for all prototypes were performed. During these tests compliance both horizontal and vertical force setup were evaluated. The boxplots show for every prototype first the original measurement and next the adjusted result. This result was used for evaluation.

Test 1.1					
Prototype	Measured displacement [mm]				
Holes	1,609	1,523	1,587	1,63	1,63
Groove	0,402	0,296	0,36	0,254	0,296
Flat	0,677	0,719	0,677	0,72	0,804
Test 1.2					
Holes	0,931	0,931	0,931	0,847	0,931
Groove	0,677	0,72	0,72	0,699	0,699
Flat	0,719	0,74	0,677	0,783	0,741
Test 1.3					
Holes	1,249	1,312	1,248	1,354	1,185
Groove	0,699	0,762	0,741	0,699	0,72
Flat	0,952	0,825	0,846	0,825	0,804
Reference					
Horizontal	0,232	0,191	0,191	0,212	0,212
Angled	0,317	0,339	0,36	0,36	0,339
Covidien SILS Clinch					
	6,2	6,052	6,2	6,56	6,475

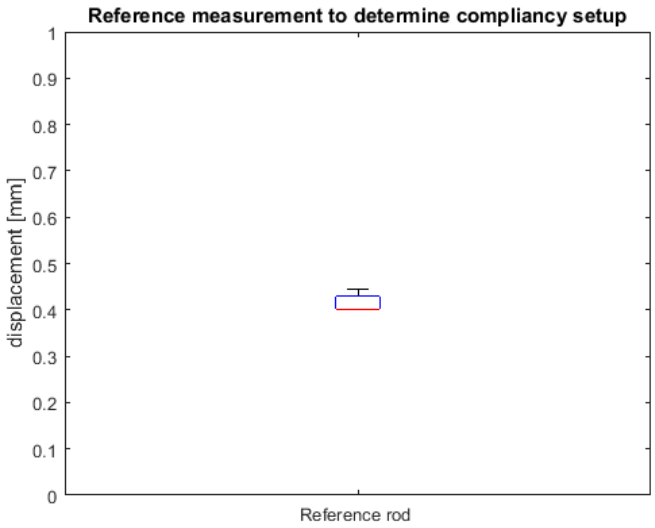

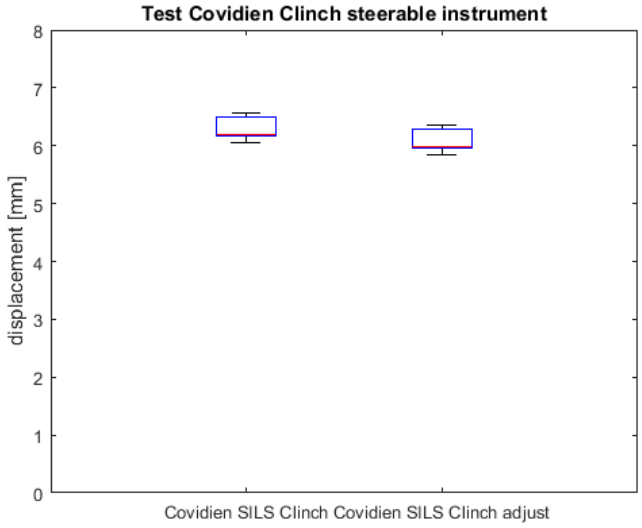

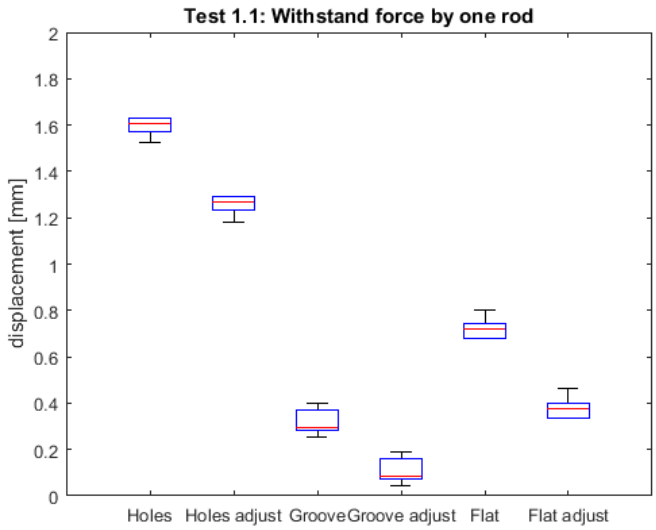

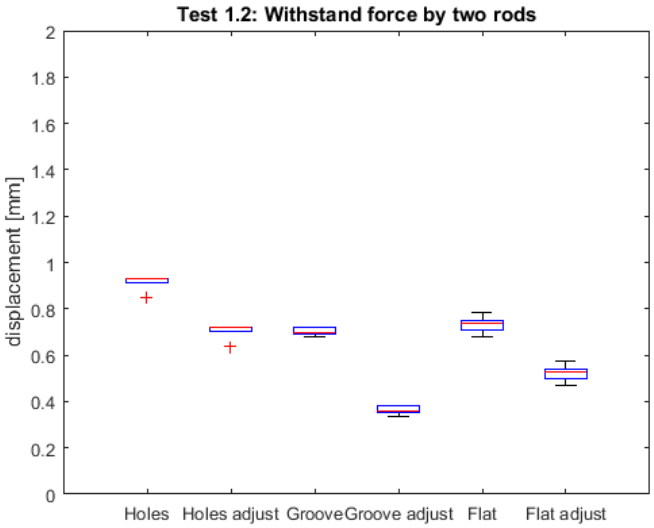

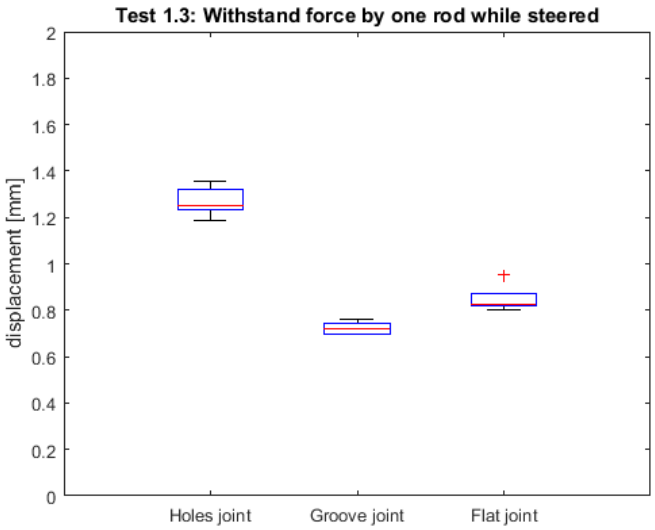

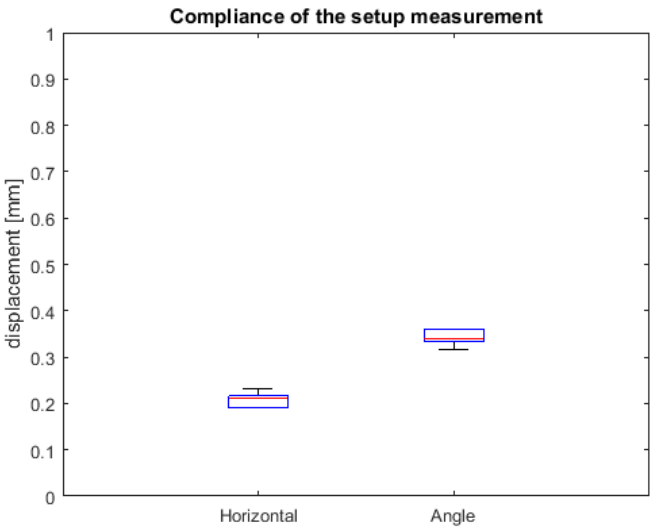

From the measuremetns was found that due to the different orientations of the force applied in one test the compliancy of the setup influences the results. In order to obtain a more reliable judgement of the stiffness of the prototypes the results were corrected for the found compliancy of the setup.

Reference measurement

Measurements were performed by measuring the displacement of a 4mm stainless steel rod. Bending of the rod itself was calculated according to the linear beam theory, shown in Equation E1, which results in a displacement of $0{,}00688mm$ while a force of $15N$ was applied. As the deformation of the rod is 53 times smaller than the measured displacement can be concluded that the measured value is caused by the compliancy in the measurement setup.

$\delta = \frac{P \cdot L^3}{3 \cdot E \cdot I}$ Used values fin the equation were: applied force $P = 15N$,free length of the beam $L = 15$mm E modulus stainless steel $E = 195.000\ MPa$ and Inertia $I = \frac{\pi}{4} \cdot r^4 = \frac{\pi}{4} \cdot 2^4$

Scaling

To scale the Groove and Flat prototype the final dimensions of the instrument the following reasoning was used. First the assumption was made that the rods only deform axial. Bending of the rods should be prevented by the frame or supports. Then the force in the rods can be scaled according to the load-displacement equation:

$$\delta_{rod} = \frac{P \cdot L}{A \cdot E} \rightarrow \delta_{scale} = \frac{2P \cdot 3L}{0{,}5^2 A \cdot E} = 24 \cdot \delta$$

The applied force P in the rods doubled to maintain static equilibrium as the moment arm of the rod towards the rotation point of the joint halves. The length of the rods was multiplied by three as the final length of the mechanism is determined to be $300mm$ instead of $100mm$ in the prototypes. As thickness of the rods halve the surface A of the rods is divided by four. Based on tis evaluation was found that the displacement of the rods now should be multiplied by a factor 24 to obtain the displacement of the rods in the final design.

In order to find the measured axial displacement of the rods in the prototypes the bending angle of joint due to the displacement is calculated. With this angle the displacement of the rod is calculated as the moment arm of the rod is known. Multiplication of this displacement with the scaling factor results in the axial displacement of the rod in the final design. The moment arm for static equilibrium of this displacement is half the moment arm of the rod in the prototype. With this displacement and moment arm the angle of rotation of the joint due to the displacement can be calculated. This is then translated back to the displacement at 15mm from the rotation point of the joint. In formulas this reasoning goes as follows:

$$\alpha_{joint\ proto} = \tan^{-1}\left(\frac{\delta_{measured\ proto}}{r_{externalforce}}\right)$$

$$\delta_{rod\ proto} = \tan(\alpha_{joint\ proto}) \cdot r_{rod\ proto}$$

$$\delta_{rod\ final} = 24 \cdot \delta_{rod\ proto}$$

$$\alpha_{joint\ final} = \tan^{-1}\left(\frac{\delta_{rod\ final}}{r_{rod\ final}}\right)$$

$$\delta_{scaled\ final} = \tan(\alpha_{joint\ final}) \cdot r_{externalforce}$$

However because the rods in the prototype were able to bend this negatively influences the achieved stiffness after scaling. Therefore the actual stiffness of the 5mm design, while rods were prevented to bend, is expected to be higher and the large difference between the Groove and Flat prototype will be eliminated.

Evaluation unexpected displacement of 1 rod versus 2 rods in the Groove and Flat prototypes.

From the stiffness tests was found that the test in which 1 rod withstands the force displaces less than the test in which 2 rods withstand the force.

First an evaluation of the working principle of concept was performed to investigate if this explains the observed behavior. As the mechanism is tested in straight orientation the rods were assumed to be loaded axially. Therefore the displacement of the rods is determined by:

$$\delta_{1rod} = \frac{P \cdot L}{A \cdot E}$$

Evaluation of this equation for the tested orientations shows that while two rods withstand the force, the surface area A doubles. The applied force however increases as the moment arm of the rods decreased and the applied external moment on the mechanism remains equal. The difference in the moment arm is determined as follows: assume that the arm is 1 of one rod withstands the force, the orientation in which two rods withstand force is rotated 45 degrees. Therefore the moment arm becomes $\cos(45) \cdot 1 = 0{,}707\ (= 0{,}5 \cdot \sqrt{2})$. To maintain static equilibrium the total force on 2 rods increases with $\frac{1}{0.707} = 1{,}41\ (= \sqrt{2})$. To compare the displacement of both orientations of the rods,

$$\delta_{2rod} = \frac{\sqrt{2} \cdot P \cdot L}{2A \cdot E}$$

This displacement is lower than while 1 rod withstands the force.

However as this was not measured, it was investigated what caused this difference from the theoretical behavior:

Comparison with Holes prototype

The Holes prototype provided the expected behavior as the measured displacement was lower when 2 rods withstand the force. The difference of the Holes principle with the Groove and Flat prototype is that rods are enclosed in the Holes prototype. Therefore rods are unable to bend. Further investigation of bending of the rods in the Groove and Flat prototypes followed.

Bending of rods

However unexpected in straight orientation of the mechanism, it could be possible that rods were bended from the surface more while 2 rods withstand forces. However evaluation of the linear beam theory does not support this. Displacement due to bending is determined by:

$$\delta = \frac{P \cdot L^3}{3 \cdot E \cdot I}$$

As the moment arm for 2 rod decreases, the total force P increases with a factor $\sqrt{2}$. However the forces were distributed over 2 rods which halves the forces in each rod. For the equation this means that the applied force on per rod while 2 rods were applied is $0{,}5 \cdot \sqrt{2}$ times the force when one rod was applied.

Moreover for the Groove prototype this is not likely to happen looking at the orientation of the grooves. If one rod withstands the force the rod is able to slide thorough the groove while bending. However if 2 rods withstand the force, the grooves have an angle of 45 degrees to the direction in which bending forces were experienced. Therefore the rods will experience more resistance by the groove.

Sliding rods due to play

As the total force on the rods is higher when two rods were applied, internal forces in the mechanism increase. Therefore, existing play between the joints in the cardan mechanism could cause that the mechanism settles and the orientation of the joint towards the rod changes. This results in play in the mechanism. When force is released the mechanism moves back to its original state and play is excluded again in straight orientation.

To verify whether this occurred during the measurements, additional tests should be performed:

1) A test in which play between joint and cardan and play between cardan and frame was eliminated.
2) A test in which displacement of the cardan is measured in the current mechanism.

Appendix F – Evaluation 5mm design

The cardan ring and joints were identified as the most vulnerable elements in the 5mm design of the instrument. In order to verify whether these elements are robust enough to withstand the forces applied to the mechanism an FEM analysis was performed. The static analysis was executed in Solidworks. After each study was verified whether the results reflect the expected behavior of the element. This was done by evaluation if the highest stresses were located at the areas in which these were expected, displacements occur in the expected directions. If the results were according to what was expected the study was approved and results used for evaluation of the elements.

First the most vulnerable element, the cardan ring was evaluated. This elements was most vulnerable in the design as all forces will be lead through this element whereas the dimensions of this element were kept small to leave enough room for maximal advantage of the Flat concept. For evaluation the cardan ring was fixated at the position of the connection with the frame stand. A force of $250N$ was applied to the position of the connections with joint. This resembles an external torque of $250Nmm$ applied to the tip resulting in a total force of $250N$ in the rods. The images below show the stresses in the material (Figure F1) and the deformation of the ring (Figure F2).

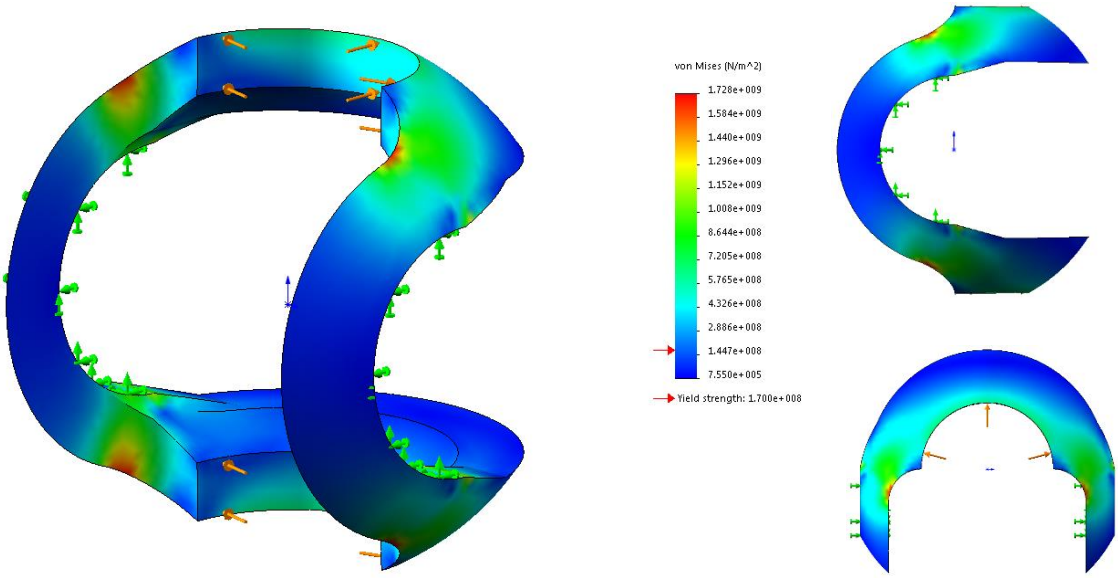

Figure F1 - Impression of the stresses in the cardan ring while a force of 250N was applied. Highest stresses of 1,72GPa were observed at the edges. Stresses in the green area are about 1GPa.

As can be seen in Figure F.1 the stresses in the material are highest at the upper and lower edges of the ring. To reduce the stresses at these points the outside the fillet can be optimized such that there is more material at that place. However should be verified that the rods will not touch the ring while the mechanism is steered to the maximal steering angle. The red arrow indicates the Yield strength of Stainless steel at $170MPa$ which is standard in Solidworks. If Maragingsteel, a 3D printable metal, was applied the Yield strength increases to $1990MPa \pm 100MPa$[1]. Then the stresses in the material then become below the yield strength. However these values for yield strength of the material should be verified for the 3D print of this element by the manufacturer.

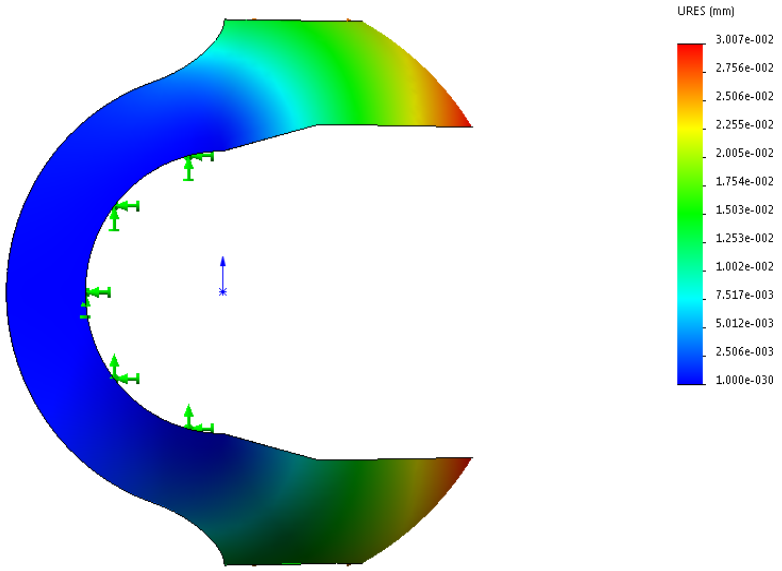

Figure F2- Impression of the displacement of the cardan ring while a force of 250N was applied. maximal displacement of the ring is 0,03mm

Maximal displacement of the ring was determined to be $0{,}03mm$. As extra space between the pin on the joint and the ring was created, the joint is still able to move. Furthermore can be observed that the displacement at the position of the connection with the hardly deforms, this means that the ring is still able to rotate with respect to the frame while the maximal force was applied.

The joint was evaluated according to the same procedure as the cardan ring. The goal of the evaluation of the joint was to determine whether no excessive forces or stresses occur in the joint while a force of 50N was applied at the distal side (where the forceps or handle is attached) while the joint was fixed. Results of the FEM analysis can be found in Figures F3 and F4.

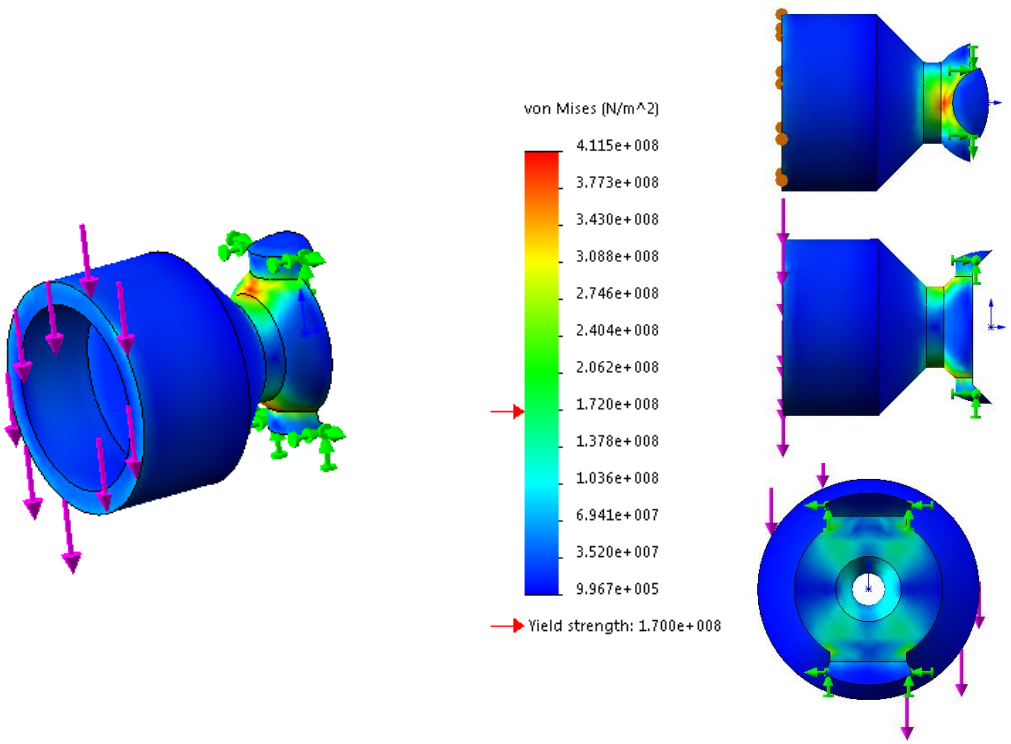

Figure F3 - Impression of the stresses in the joint while a force of 50N was applied to the distal side of the joint. Maximal stresses of 411MPa were observed in the transitions of spherical part and pin.

Evaluation of the results showed as expected that highest stresses occur at the transitions between the spherical part and the pins on top and bottom and pin at the back. By optimization of this part of the joint the stresses could be minimized. However if the joint is printed in Stainless steel 316L (Yield strength $530MPa \pm 60MPa$[1]) or Maragingsteel the stresses will remain below the yield strength and no plastic deformation will occur.

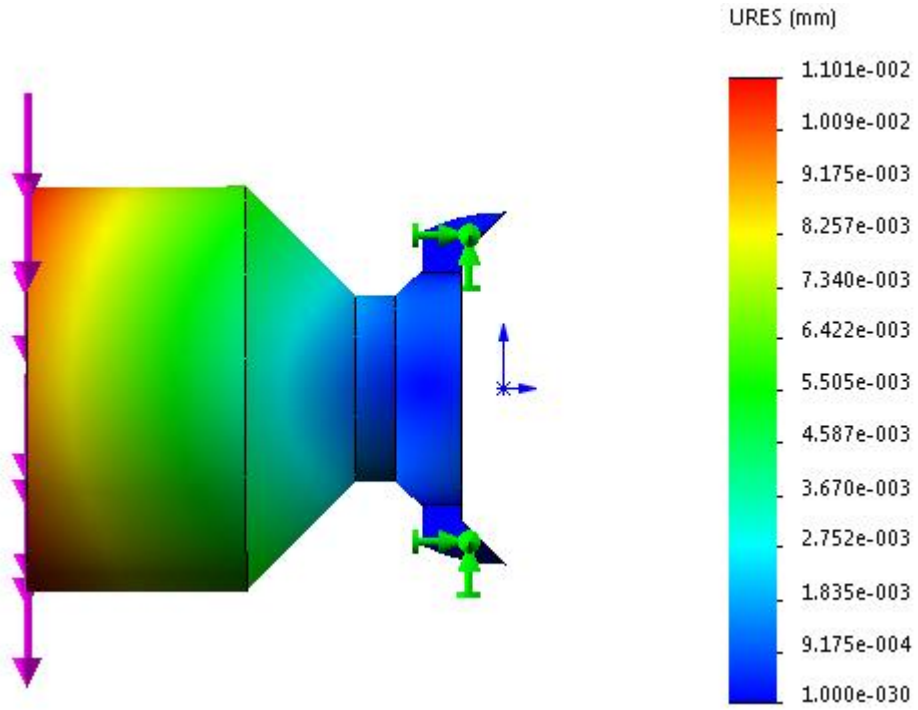

Figure F4 - Impression of the deformation of the joint while a force of 50N was applied. Maximal deformation was 0,01mm.

Deformation of the joint is maximally 0,01mm. As a result the deformation at 15mm from the rotation point of joint will be approximately 0,03mm.

The rods will be designed such that the rods were unable to bend. Therefore the rods were not evaluated in this simulation. Axial displacement of the rods in the final design is determined by the load displacement equation:

$$\delta_{rod} = \frac{P \cdot L}{A \cdot E} = \frac{250 \cdot 300}{\pi \cdot 0{,}5^2 \cdot 195E^9} = 0{,}49mm$$

[1] Specifications of the materials were obtained from the website of Oceanz, a 3D print company capable of printing parts in these materials. http://www.oceanz.eu/metalen Website visited 20-20-2017.